General Disclaimer

One or more of the Following Statements may affect this Document

- This document has been reproduced from the best copy furnished by the organizational source. It is being released in the interest of making available as much information as possible.

- This document may contain data, which exceeds the sheet parameters. It was furnished in this condition by the organizational source and is the best copy available.

- This document may contain tone-on-tone or color graphs, charts and/or pictures, which have been reproduced in black and white.

- This document is paginated as submitted by the original source.

- Portions of this document are not fully legible due to the historical nature of some of the material. However, it is the best reproduction available from the original submission.

PLASMA PHYSICS GROUP

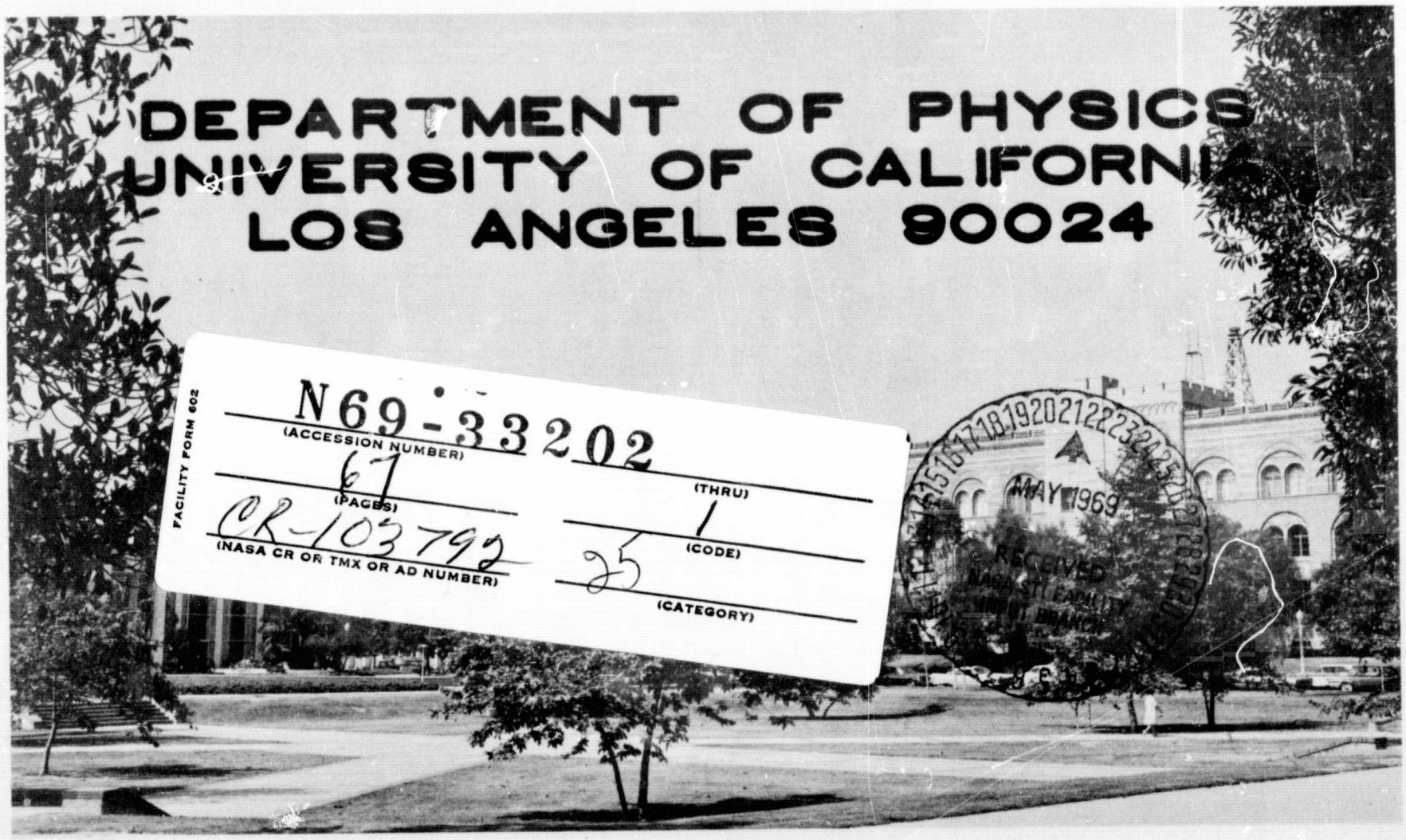

Parametric Mode-Mode Coupling Between Drift Waves in Plasmas

Francis Hai and Alfred Y. Wong

January 1969 R-40

Plasma Physics Group
Department of Physics
University of California
Los Angeles, California

This research was supported by funds from NASA Grant No. NGR-05-007-066.

Parametric Mode-Mode Coupling Between Drift Waves in Plasmas*

Francis Hai and Alfred Y. Wong

Department of Physics, University of California, Los Angeles, California

ABSTRACT

The nonlinear phenomenon of parametric excitation of stable resonant drift modes through mode-mode coupling is examined in the potassium plasma of a Q device. The scheme investigated extensively is the degenerate case of three-mode parametric coupling in which the stable resonant mode (m=1) at ω_1 is excited by the externally driven pump mode (m=2) at $\omega_0 = 2\omega_1$. The usual frequency and wave number matching conditions are satisfied. The additional, new aspects examined are the enhancement of thermal fluctuations, the threshold for excitation, and the power balance between the coupled modes and the external source. The main results obtained are the measurement of the coupling coefficient and the determination of the functional behavior of the modes. General agreement between the experimental results and theory derived from the expansion of the governing fluid equations to second order is attained. To describe the steady state amplitudes observed experimentally, nonlinear saturation phenomena are included. Nondegenerate and higher order coupling schemes are briefly considered. Parametric coupling as a mechanism limiting the amplitude of an unstable mode and leading to a turbulent plasma is presented and discussed.

---

* This research was supported by the National Aeronautics and Space Administration Grant No. NGR05-007-066 and is part of a dissertation submitted by F. Hai in partial fulfillment of the requirements for the degree of Doctor of Philosophy in Physics at the University of California, Los Angeles.

I. INTRODUCTION

Waves in the nonlinear regime can couple in a number of ways among which the most efficient is the regenerative coupling involving resonant modes. A fully-ionized plasma is a particularly attractive medium for the investigation of such a coupling process because only two components are involved--ions and electrons; the accessibility to internal probing makes it possible to measure thermal fluctuations and local parameters, permitting a quantitative functional identification of the parametric coupling process. Recent interest stems not only from the need for a basic understanding of this process but also from its possible role in limiting the amplitude of an unstable mode as well as establishing a turbulent plasma.

Parametric coupling as examined in this paper involves the interaction between a "pump" drift mode of finite amplitude at frequency ω_0 and fluctuating drift modes at frequencies ω_1 and ω_2 present in the thermal noise spectrum. This nonlinear interaction under the optimum frequency matching condition $\omega_0 = \omega_1 + \omega_2$ enhances the fluctuations about ω_1 and ω_2. The enhanced fluctuations in turn interact with the pump, and this regenerative process continues, eventually yielding coherent, steady state, and finite amplitude drift modes at these two frequencies. Two main results emerge from our experimental and theoretical investigation--a quantitative description of the parametric process starting from the thermal fluctuating level and a measurement for the first time of the parametric mode-mode coupling coefficient in plasma.

Numerous experimental studies of parametric interaction in plasmas

involving electron plasma and ion acoustic waves, lower hybrid oscillations and the upper hybrid resonance, and others have been reported.[1] Although most of these studies satisfied the necessary condition for parametric coupling, that of frequency matching, i.e., $\omega_0 = \omega_1 + \omega_2$ (however not a sufficient one because a simple beating process also satisfies this condition), and measured a definite threshold for excitation, positive identification of parametric coupling has not been possible because the measured threshold values do not agree with those predicted theoretically. In this paper we report additional, new aspects, besides the threshold value, which serve to identify the parametric mode-mode coupling process. Among these are (1) the enhancement of thermal fluctuations about the parametrically excited mode, (2) the variation of the threshold with the frequency of the pump, (3) the phase between the pump and the excited mode which together with the threshold determines completely the coupling coefficient, (4) the conservation of power in the parametric process, and (5) the steady state behavior of both the pump and the excited mode above threshold. Agreement between the experimental results and theory is attained for many of these aspects.

The parametric process described extensively in this paper is examined in a stable plasma in which the pump mode is externally excited. However, we have also observed in an unstable plasma in the absence of external excitation what appears to be parametric coupling to a lower mode by an unstable mode. This process which limits the amplitude of the unstable mode exhibits many of the characteristics of the stable regime such as frequency matching, enhancement from fluctuations, and

phase variation between the pump and the excited mode. By successive mode coupling, a single unstable mode can evolve into a multi-mode or a turbulent spectrum.

Recent theoretical interest in parametric coupling was initiated by Silin[2] and by DuBois and Goldman.[3] Using the fluid equations for a cold plasma, Silin demonstrated the possibility of exciting electron plasma waves by an external oscillating electric field. DuBois and Goldman, and subsequently others,[3] considered coupling between the electron plasma mode and the highly damped ion acoustic mode by either an external transverse electromagnetic wave or a longitudinal wave. A particularly important aspect of the work by DuBois and Goldman is their treatment of the thermal noise spectrum in the parametric process, a method we have followed in our explanation of the enhancement of the drift wave fluctuation spectrum. Parametric excitation involving transverse electromagnetic waves, ion plasma oscillations, and other types of plasma waves have been investigated theoretically.[4] Since the report of experimental observation of parametric coupling between drift waves,[5] detailed theory describing this latter process has been given by Weyl and Goldman[6] and Stix.[7]

All previous experimental studies of parametric interaction in plasma have been conducted in discharge type plasmas. The experiment described here involving density gradient driven drift waves is performed in the highly ionized plasma of a Q device.[8] The drift wave is an electrostatic mode occurring in a plasma possessing inhomogeneity in density. This instability is observed as a low-frequency density and potential perturbation propagating in the region of maximum density

gradient of the plasma in a magnetic field. In the cylindrical plasma of a Q device drift waves are essentially ion acoustic waves propagating azimuthally, almost perpendicular to the axial magnetic field ($k_\phi >> k_z$) . The periodicity of the wave in the azimuthal direction gives rise to resonant modes with integral relationship $k_\phi = m/r_0$ where m is the integral azimuthal mode number and r_0 is the radius at which the mode is observed. The regenerative nature of parametric coupling between these modes is depicted in Fig. 1. An external signal excites a drift mode at frequency ω_0 in a stable plasma. This pump mode interacts with fluctuating drift modes at frequencies ω_1 and ω_2 in the thermal spectrum. When the frequency matching condition is satisfied, $\omega_0 = \omega_1 + \omega_2$, the pump mode couples the two thermal modes and enhances their fluctuating spectrum through feedback action occurring at $\omega_0 - \omega_1$ and $\omega_0 - \omega_2$. The coupling scheme most easily observed experimentally and investigated in this paper is that in which the $m = 1$ drift mode at ω_1 is parametrically excited by an externally excited $m = 2$ mode at ω_0 . This coupling scheme is also described by the diagram in Fig. 1, being a degenerate case of three-mode coupling in which $\omega_1 = \omega_2$.

Drift waves are ideal for the study of parametric mode-mode coupling in plasmas because (1) the "pump" mechanism is another drift mode whose amplitude and frequency may be controlled externally,[9] (2) the damping associated with a drift mode may be varied arbitrarily close to marginal stability by varying a parameter of the system such as the magnetic field, (3) the damping of the excited mode which is related to the threshold for parametric excitation may be experimentally

determined,[9] and (4) drift waves satisfy approximately the linear dispersion relation $\omega = k V_D$ and therefore meet the matching conditions for propagating waves in parametric coupling

$$\omega_0 = \omega_1 + \omega_2 \quad , \qquad k_0 = k_1 + k_2$$

(for the degenerate case $\omega_1 = \omega_2$, $k_1 = k_2$). These attributes of drift waves have made possible the detailed study of the parametric process.

This paper restricts itself mainly to three-mode parametric coupling of drift waves. For quantitative comparison, the theoretical results are evaluated for the degenerate case for which extensive experimental data are available. However, a brief experimental examination of nondegenerate three-mode coupling and four-mode coupling is included. The theory of parametric coupling presented follows closely that given in an earlier paper[10] and that reported by Weyl and Goldman.[6] Some of the experimental results given here have been published earlier.[10]

In Sec. II, the theory describing parametric coupling between drift waves is reviewed. Section III describes the experimental arrangement used in this study. In Sec. IV, a comparison between the experimental data and the theory developed in Sec. II is given and discussed. Section V contains the conclusions.

II. THEORY

The theory of parametric mode-mode coupling of drift waves is reviewed in this section. First, the basic theory from a fluid description of the plasma is briefly outlined in Sec. IIA. A nonlinear dispersion relation describing the excited mode is obtained. To extract useful analytical expressions for comparison with experimentally measured quantities, a resonance approximation is assumed in Sec. IIB for the linear dielectric function contained in the nonlinear dispersion relation.

Following the development of the parametric process as observed experimentally, we examine first the coupling of the pump and the excited mode below threshold in Sec. IIC. In order to describe the process in this regime, thermal fluctuations are included in the theory. The spectral power density, the peak power density, and the total integrated power describing the regenerative enhancement of fluctuations are derived with this consideration. In addition, the balance of power between the coupled modes and the external source is examined. Some of the results given in this section have been reported earlier[10] and obtained by Weyl and Goldman.[6] Extending the theory into the regime at and above threshold, we have obtained additional results.

In the regime beyond the threshold, we simplify our consideration of the mode coupling process in Sec. IID with the neglect of thermal fluctuations, an approximation justified by the now enhanced amplitude and coherent phase of the excited mode. This regime is described by the nonlinear dispersion relation derived in Sec. IIA. The solution of

this relation yields the frequency and the growth rate, the threshold, and the coupling coefficient. In addition, the phase between the pump and the excited mode is derived in this section.

Above the threshold and under steady state conditions, the amplitude of the excited mode saturates at a finite value. This saturation results from finite power input and changes in zero order conditions occurring with finite amplitude drift modes. In Sec. IIE, we assume that the mechanisms leading to the observed steady state amplitude of the excited mode is the change in the density gradient and incoherent wave-particle scattering[11] associated with drift wave induced diffusion.

A. The Basic Theory

A description of the coupling process is derived from the nonlinear Poisson's equation which determines the fluctuating plasma potentials and which is developed with a fluid model of the plasma. The basic equations governing density gradient drift waves are the electron and ion equations of motion, the continuity equation, and Poisson's equation:

$$0 = -\frac{e}{m_e}\left(\underset{\sim}{E} + \frac{\underset{\sim}{v} \times \underset{\sim}{B}}{c}\right) - \frac{1}{nm_e}\underset{\sim}{\nabla P} - \frac{\eta_z e^2}{m_e} n\underset{\sim}{v}_z = 0 \tag{1}$$

$$\frac{d}{dt}\underset{\sim}{v}_\perp - \frac{1}{4}\rho_i^2\,\underset{\sim}{v}_{ii}\,\nabla^2\,\underset{\sim}{v}_\perp = \frac{e}{m_i}\left(\underset{\sim}{E} + \frac{\underset{\sim}{v} \times \underset{\sim}{B}}{c}\right) - \frac{1}{nm_i}\underset{\sim}{\nabla P} \tag{2}$$

$$\frac{\partial n}{\partial t} + \underset{\sim}{\nabla} \cdot (n\underset{\sim}{v}) + \sigma n = 0 \tag{3}$$

$$\underset{\sim}{\nabla} \cdot \underset{\sim}{E} = 4\pi e(n_i - n_e) \tag{4}$$

The notation used is the usual one and is defined below. For mathematical simplicity the fluid model assumed is solved in rectangular coordinates.[12] The following are assumed for the model described by the equations above: (a) the plasma is in a uniform magnetic field $\underset{\sim}{B}$ in the Z direction; (b) the variation of the zero order density is exponential in the X direction, $-\frac{1}{n}\frac{\partial n}{\partial x} = \kappa$ = constant, as observed over the region where the wave exists; (c) the waves are electrostatic, $\underset{\sim}{E} = -\underset{\sim}{\nabla}\phi$, with $k_y >> k_z$; (d) electron inertia is neglected; (e) the basic mechanisms governing the drift instability-- ion inertia, finite Larmor radius ρ_i $(0 < k_y\rho_i << 1)$, and electron resistivity η_z along $\underset{\sim}{B}$ --are included; (f) ion viscosity in the form $\frac{1}{4}\rho_i^2 \nu_{ii} \nabla^2 \underset{\sim}{v}_\perp$ is assumed[13]; (g) ion motion along $\underset{\sim}{B}$ is neglected since $V_e >> \omega/k_z >> V_i$ where V_e and V_i are the thermal velocities of the electrons and the ions, respectively, and ω/k_z is the phase velocity of the wave along $\underset{\sim}{B}$; (h) the wave frequency is much less than the ion cyclotron frequency, $\omega << \omega_{ci}$; (i) the quantity σ is included to account for phenomenological losses, e.g., losses at the boundary, the end plates of the Q device; and (j) varying quantities have the functional form $\exp[i(k_y y + k_z z - \omega t)]$ and are independent of x.

Expansion of Eqs. (1) through (3) to second order in the excited field $e\phi/KT$, where K is Boltzmann's constant and T is the temperature of both the electrons and the ions, shows that the coupling of the drift modes arises from electron mobility parallel to $\underset{\sim}{B}$, $(\eta_z e^2/m_e)\, n v_{\sim z}$, the ion mobility transverse to $\underset{\sim}{B}$, $\frac{1}{4}\rho_i^2 \nu_{ii} \nabla^2 \underset{\sim}{v}_\perp$, and the pressure of the particles, $(1/m_e n)\, \underset{\sim}{\nabla}P$, $(1/m_i n)\, \underset{\sim}{\nabla}P$ $(P = nKT)$.[14] This mode-mode coupling process alters the linear

stability conditions[13] for drift modes and could cause a mode to go unstable. This new stability condition which includes the parametric coupling is described by the nonlinear dispersion relation derived below.

Poisson's equation including mode-mode coupling takes the following form[6,10]

$$\varepsilon^{L}(\underset{\sim}{k}_1,\omega_1)\Phi_1(\underset{\sim}{k}_1,\omega_1) + \Phi_0 \, M \, \Phi_1(\underset{\sim}{k}_1-\underset{\sim}{k}_0,\omega_1-\omega_0) = 0 \tag{5}$$

$$\varepsilon^{L}(\underset{\sim}{k}_1-\underset{\sim}{k}_0,\omega_1-\omega_0)\ \Phi_1(\underset{\sim}{k}_1-\underset{\sim}{k}_0,\omega_1-\omega_0) + \Phi_0 \, M^{*} \, \Phi_1(\underset{\sim}{k}_1,\omega_1) = 0 \tag{6}$$

where $\varepsilon^{L}(\underset{\sim}{k}_1,\omega_1)$ is the linear dielectric function for the excited mode, $\Phi_0 = e\phi_0/KT$ the dimensionless amplitude of the pump wave potential, $\Phi_1 = e\phi_1/KT$ the excited wave potential, and M, a dimensionless matrix element, represents the coupling between the pump mode and the excited mode. The effects of parametric coupling appearing explicitly in our discussion of enhancement of fluctuations and threshold for excitation are embodied in the nonlinear dielectric function $\varepsilon^{NL}(\underset{\sim}{k}_1,\omega_1,\Phi_0)$ which is obtained by eliminating $\Phi_1(\underset{\sim}{k}_1-\underset{\sim}{k}_0,\omega_1-\omega_0)$ from Eqs. (5) and (6), yielding

$$\varepsilon^{NL}(\underset{\sim}{k}_1,\omega_1,\Phi_0)\Phi_1(\underset{\sim}{k}_1,\omega_1) = 0$$

$$\varepsilon^{NL} = \varepsilon^{L}(\underset{\sim}{k}_1,\omega_1) - \frac{\Phi_0^{\,2}\,|M|^2}{\varepsilon^{L}(\underset{\sim}{k}_1-\underset{\sim}{k}_0,\omega_1-\omega_0)} = 0 \quad . \tag{7}$$

Equation (7), the nonlinear dispersion relation, is quite general and is descriptive of any case of electrostatic three-mode coupling. We now proceed to find an explicit expression of ε^{NL} for drift waves.

B. The Resonance Approximations

The linear dispersion relation describing the excited mode in the absence of coupling ($M = 0$ or $\Phi_0 = 0$) is

$$\epsilon^L(\underset{\sim}{k}_1, \omega_1) = 0 \quad . \tag{8}$$

Equation (8) derived from the linear expansion of Eqs. (1) through (4) is a quadratic equation in ω.[13] For the conditions occurring experimentally, the drift mode of interest given by the solution of Eq. (8) for $\omega_1 = \Omega + i\Gamma$ is[15]

$$\Omega = k_y V_D \{1 - C_\Omega\} \tag{9}$$

$$\Gamma = - \{\sigma - \Gamma_g(2 - C_\Gamma)\} \tag{10}$$

where

$$\Gamma_g = \frac{(k_y V_D)^2 (k_y \rho_i)^2}{k_z^2 V_e^2 / \nu_{ei}} \quad .$$

V_D is the electron diamagnetic drift velocity defined by $V_D = (V_i^2/\omega_{ci})\,\kappa$; C_Ω and C_Γ are the correction factors for the frequency and the damping, respectively. Both are primarily dependent on the effects of finite Larmor radius $(k_y\rho_i)^2$, ion diffusion transverse to $\underset{\sim}{B}$ resulting from ion-ion collisions ν_{ii}, $[\frac{1}{4}(k_y\rho_i)^4\,\nu_{ii}]$, and electron diffusion along $\underset{\sim}{B}$ associated with electron-ion collisions ν_{ei}, $(k_z^2 V_e^2/\nu_{ei})$. Γ_g is the usual growth factor computed from the linear theory of density gradient drift waves.

Equations (9) and (10) describe a drift mode propagating in the electron diamagnetic drift direction with velocity somewhat less than V_D. Application of Eq. (9) to the cylindrical plasma of the Q device

($k_y = m/r_0$) reveals discrete drift modes which are integrally related if the correction factor C_Ω is negligible. Under this condition the frequency and wave number matching required for parametric coupling is easily satisfied. For the temporal variation assumed, $e^{-i\omega t}$, Eq. (10) states that the mode is stable ($\Gamma < 0$) for sufficiently large values of Larmor radius ρ_i, ion-ion collisions ν_{ii}, and/or end-plate losses σ. This is the regime in which most of the experiments described in this paper are performed.

The complexity of this linear dielectric function $\varepsilon^L(\underset{\sim}{k}_1,\omega_1)$ makes the nonlinear dispersion relation, Eq. (7), particularly difficult to solve. However, because parametric coupling observed experimentally is mainly between resonant modes, $\varepsilon^L(\underset{\sim}{k}_1,\omega_1)$ may be replaced by its resonance approximation which simplifies considerably the analysis and understanding of the nonlinear dielectric function. With the assumption that each mode of interest is near a zero of the linear dispersion relation, expansion of ε^L about this zero yields

$$\varepsilon^L(\underset{\sim}{k}_1,\omega_1) \simeq \frac{[\omega_1 - (\Omega + i\Gamma)]}{\delta\Omega} + 0\left[\frac{\omega_1 - (\Omega + i\Gamma)}{\Omega}\right]^2 \qquad (11)$$

where

$$\delta^{-1} = \Omega \left.\frac{\partial\varepsilon^L(\underset{\sim}{k}_1,\omega_1)}{\partial\omega_1}\right|_{\omega_1=\Omega+i\Gamma}$$

and

$$\varepsilon^L(\underset{\sim}{k}_1, \Omega + i\Gamma) = 0 \quad .$$

Evaluation of Eq. (11) gives

$$\varepsilon^L(\underset{\sim}{k}_1,\omega_1) \simeq \frac{k_D^2}{k_1^2}\left\{\frac{\omega_1 - (\Omega + i\Gamma)}{\Omega}\right\} \tag{12}$$

$$\varepsilon^L(\underset{\sim}{k}_1-\underset{\sim}{k}_0,\omega_1-\omega_0) \simeq \frac{k_D^2}{(k_1-k_0)^2}\left\{\frac{(\omega_1-\omega_0) - (\Omega + i\Gamma)}{\Omega}\right\} \tag{13}$$

where Ω and Γ are defined by Eqs. (9) and (10), respectively. We observe that $\varepsilon^L(\underset{\sim}{k}_1-\underset{\sim}{k}_0,\omega_1-\omega_0) = \varepsilon^L(\underset{\sim}{k}_1,\omega_1)^*$ for $\underset{\sim}{k}_0 = 2\underset{\sim}{k}_1$ and $\omega_0 = 2\omega_1$, the case of experimental concern.

The nonlinear dispersion relation is simplified further by the fact that the coupling factor M is not a sensitive function of frequency and can be approximated by its value at the resonance Ω. M [obtained with the derivation of Eq. (5)] is[6]

$$M \simeq \frac{k_D^2}{k_1^2}\left\{-4(k_y\rho_i)^2 - i\,8\,\frac{(k_yV_D)(k_y\rho_i)^2}{k_z^2V_e^2/\nu_{ei}}\right\} . \tag{14}$$

The terms in M involving ν_{ii} have been omitted, being negligibly small for the regime investigated experimentally.

Substitution of Eqs. (12), (13), and (14) into the nonlinear dispersion relation in Eq. (7) gives

$$(\omega_1-\Omega-i\Gamma)(\omega_1-\omega_0+\Omega-i\Gamma) + \Phi_0^2(k_1^2/k_D^2)^2\,\Omega^2\,|M|^2 = 0 \tag{15}$$

where $\Omega(\underset{\sim}{k}_1-\underset{\sim}{k}_0) = -\Omega(\underset{\sim}{k}_1)$ as implied by Eq. (9) has been used. The solution of Eq. (15) for $\omega_1 = \omega_R + i\gamma$ is

$$\omega_R = \omega_0/2 \tag{16}$$

$$\gamma = \Gamma + \left\{\Phi_0^2 \left(\frac{k_1^2}{k_D^2}\right)^2 \Omega^2 |M|^2 - \left(\frac{\omega_0}{2} - \Omega\right)^2\right\}^{1/2} \qquad (17)$$

where ω_R is half the pump frequency as expected and γ is the growth rate of the parametrically excited mode; Γ is the linear damping rate of the mode in the absence of parametric coupling. Equation (17) shows that the threshold for parametric excitation ($\gamma = 0$) is dependent not only on the pump amplitude but also on the pump frequency. For a stable plasma ($\Gamma < 0$), the minimum threshold occurs when the frequency of the pump ω_0 is twice the resonant frequency of the excited mode Ω and is given by

$$\Phi_M = -\frac{\Gamma/\Omega}{\frac{k_1^2}{k_D^2}|M|} \quad . \qquad (18)$$

With this derivation of the minimum threshold, we are now ready to examine parametric excitation starting from the thermal fluctuating level.

C. The Fluctuation Spectrum

In this experiment where parametric excitation occurs with the introduction of only one coherent signal, the pump, the process must be initiated by the coupling of this pump with thermal fluctuations. These fluctuations are included as additional source terms in the Poisson's equations (5) and (6):

$$\epsilon^L(\underset{\sim}{k},\omega)\ \Phi_1(\underset{\sim}{k},\omega) + \Phi_0\ M\ \Phi_1(\underset{\sim}{k}-\underset{\sim}{k}_0,\omega-\omega_0) = \frac{4\pi e}{KT\ k^2}\rho_{f1}(\underset{\sim}{k},\omega) \qquad (19)$$

$$\varepsilon^L(\underset{\sim}{k}-\underset{\sim}{k}_0,\omega-\omega_0)\ \Phi_1(\underset{\sim}{k}-\underset{\sim}{k}_0,\omega-\omega_0) + \Phi_0\ M^*\ \Phi_1(\underset{\sim}{k},\omega) =$$

$$= \frac{4\pi e}{KT|\underset{\sim}{k}-\underset{\sim}{k}_0|^2}\ \rho_{fl}(\underset{\sim}{k}-\underset{\sim}{k}_0,\omega-\omega_0) \qquad (20)$$

where $\rho_{fl}(\underset{\sim}{k},\omega)$ is the thermal fluctuating charge density and is related to $\varepsilon^L(\underset{\sim}{k},\omega)$ through the fluctuation-dissipation theorem. For a stable system in a nonequilibrium steady state (e.g., a plasma with a density gradient), with mode coupling ignored, a formal extension of this theorem gives[16]

$$\lim_{V,\tau\to\infty} \frac{\langle|\rho_{fl}(\underset{\sim}{k},\omega)|^2\rangle}{V\tau} = \frac{k^2\ KT\ f(\underset{\sim}{k},\omega)\ \mathrm{Im}\ \varepsilon^L(\underset{\sim}{k},\omega)}{2\pi\omega} \qquad (21)$$

where V is the volume of the system, τ is time, and $f(\underset{\sim}{k},\omega)$ is a form factor arising from the condition of nonequilibrium. For a system in equilibrium, $f = 1$. With Eqs. (19), (20), and (21), expressions for several quantities measured experimentally in this regime below threshold may be derived.

(i) The spectral power density.

The quantity of interest in the measurement of fluctuations is the spectral power density $S(\underset{\sim}{k},\omega)$ which describes a distribution in both frequency and wave number. The wave numbers are restricted to nearly discrete values $(k = m/r_0)$ because of the cylindrical geometry of the plasma and are spatially analyzed by the method involving several probes displaced azimuthally as described in Sec. III. The spectral power density $S(\omega)$ obtained by integration over k in the neighborhood of

a discrete wave number k_1 becomes

$$S(\omega) = \int_{k_1} d^3k\, S(\underset{\sim}{k},\omega) = \frac{\Delta^3 k_1}{(2\pi)^3} S(\underset{\sim}{k}_1,\omega)$$

$$= \lim_{V,\tau\to\infty} \frac{\Delta^3 k_1}{(2\pi)^3} \frac{<|\Phi(\underset{\sim}{k}_1,\omega)|^2>}{V\tau} \quad .$$

To evaluate $S(\omega)$ an expression for $\Phi(k,\omega)$ is obtained from Eqs. (19) and (20).

$$\Phi(\underset{\sim}{k}_1,\omega) = \frac{4\pi e}{KT\, k_1^2} \frac{[\varepsilon^L(\underset{\sim}{k}_1-\underset{\sim}{k}_0,\omega-\omega_0)\ \rho(\underset{\sim}{k}_1,\omega) - M\ \Phi_0\ \rho(\underset{\sim}{k}_1-\underset{\sim}{k}_0,\omega-\omega_0)]}{\varepsilon^L(\underset{\sim}{k}_1-\underset{\sim}{k}_0,\omega-\omega_0)\ \varepsilon^{NL}(\underset{\sim}{k}_1,\omega,\Phi_0)} \quad .$$

With the definitions above, the spectral power density associated with the excited mode is obtained:

$$S(\omega) = \frac{\Delta^3 k_1}{(2\pi)^3} \frac{2\Gamma f}{n} \frac{(\omega-\Omega)^2 + \Gamma^2\left(1 + (\Phi_0^2/\Phi_M^2)\right)}{[(\omega-\Omega)^2 + \Gamma^2\left(1 + (\Phi_0/\Phi_M)\right)^2][(\omega-\Omega)^2 + \Gamma^2\left(1-(\Phi_0/\Phi_M)\right)^2]} \tag{22}$$

We note that $f(\underset{\sim}{k}_1,\omega)$, the form factor, may cause an asymmetry in the observed frequency spectrum $S(\omega)$. Φ_M is the minimum threshold pump amplitude defined explicitly in Eq. (18). $S(\omega)$ given above describes the enhanced spectrum near the resonant frequency Ω. The spectrum narrows and increases in amplitude as the pump amplitude Φ_0 approaches the threshold Φ_M, a consequence of the feedback process described in Fig. 1.

(ii) The peak power density.

The enhanced spectrum peaks at the resonant frequency Ω and can be expressed in a particularly simple form. This peak amplitude is easily obtained from Eq. (22) and related to the value without mode coupling (M = 0):

$$S(\Omega) = S_{M=0} \frac{[1 + (\Phi_0^2/\Phi_M^2)]}{[1 - (\Phi_0^2/\Phi_M^2)]^2} \tag{23}$$

where

$$S_{M=0} = \frac{\Delta^3 k_1}{(2\pi)^3} \frac{2}{n} \frac{f}{\Gamma} \quad .$$

The peak power rises rapidly as the pump amplitude approaches the threshold Φ_M.

(iii) The total, integrated power.

The total power associated with the enhanced spectrum around Ω obtained from Eq. (22) is

$$\int \frac{d\omega}{2\pi} S(\omega) \simeq \frac{[1 + (\Phi_0^2/\Phi_M^2)]}{[1 + (\Phi_0/\Phi_M)][1 - (\Phi_0^2/\Phi_M^2)]} \int \frac{d\omega}{2\pi} S_{M=0}(\omega) \tag{24}$$

where

$$S_{M=0}(\omega) = \frac{\Delta^3 k_1}{(2\pi)^3} \frac{2}{n} \frac{\Gamma f}{(\omega-\Omega)^2 + \Gamma^2} \quad .$$

Comparison of Eqs. (23) and (24) shows that the normalized peak power density rises more rapidly than the normalized integrated power spectrum. As a consequence of our perturbative procedure the expressions derived above are valid only for $\Phi_0 < \Phi_M$. Near Φ_M higher order effects

must be considered.

A more general criterion for parametric enhancement which must be satisfied in both the linear and nonlinear regime is the conservation of power. In fact, the enhanced fluctuation spectrum cannot be arbitrarily large precisely because of the limited power available. A computation of the power dissipated by the coupled modes with second order terms can be obtained.

(iv) The balance of power.

The total power per unit volume expended by the external driving source is[6]

$$\frac{P_{EX}}{V} = \frac{1}{V}\int d\underset{\sim}{r}\ \langle \underset{\sim}{J}\cdot\underset{\sim}{E}\rangle$$

$$= 2\,k_D^{\,2}\,\Gamma_0\,\phi_0^{\,2} + 2\,k_D^{\,2}\,\Gamma\,\frac{(KT)^2}{e^2}\int\frac{d\omega}{2\pi}\,[S(\omega) - S_{M=0}(\omega)]\ . \quad (25)$$

The first term on the right hand side represents the dissipation of the pump mode while the second term represents that of the fluctuation spectrum enhanced over and above the thermal fluctuations. A diagram schematically representing Eq. (25) is given in Fig. 2. The power dissipated in the plasma by each mode is proportional to its damping factor Γ. Initially, the input power is totally dissipated by the pump mode. However, as the fluctuation spectrum around the excited mode frequency is enhanced, the pump amplitude must decrease in order to conserve energy. As the amplitudes of the modes increase into the nonlinear regime, appropriate nonlinear damping rates Γ and Γ_0 must be used. These rates have been calculated in a separate paper

where single nonlinear modes are considered.[17] A check of the power balance is a necessary procedure in order to ensure that energy is not channeled into modes other than those considered.

D. The Threshold and the Coupling Coefficient

The description of the parametric process derived in the preceding section is valid only below threshold, $\Phi_0 < \Phi_M$. However, as Φ_0 approaches Φ_M the amplitude of the excited mode greatly exceeds the thermal fluctuating level and the phase becomes coherent with respect to that of the pump. In this regime near threshold, the thermal fluctuating charge densities in Eqs. (19) and (20) may be neglected. The coupling is now described by the solution of the nonlinear dispersion relation given by Eqs. (16) and (17). Several important aspects of parametric coupling are given by this solution.

(i) The frequency and growth rate of the excited mode.

Equation (16) states that the excited mode frequency is exactly half the pump frequency, $\omega_R = \omega_0/2$. Equation (17) describes the stability of the excited mode. This mode was assumed to be normally damped, $\gamma < 0$. However, this mode becomes excited and grows if either Φ_0 the pump amplitude or M the coupling factor is sufficiently large as to overcome the linear damping Γ. As expected intuitively, the growth rate is a maximum when the frequency of the excited mode $(\omega_0/2)$ coincides with a natural resonance of the system (Ω).

(ii) The threshold.

With the pump applied at a frequency ω_0, the parametric threshold

is defined as the minimum amplitude of the pump at which the excited mode becomes marginally stable ($\gamma = 0$). From Eq. (17) this occurs at

$$\Phi_C = \left\{ \frac{\Gamma^2 + [(\omega_0/2)-\Omega]^2}{(k_1^2/k_D^2)^2\ \Omega^2\ |M|^2} \right\}^{1/2} \quad . \tag{26}$$

This expression indicates that the threshold for excitation Φ_C increases as the excited mode frequency shifts from resonance (achieved experimentally by varying the pump frequency ω_0). Conversely, the frequency zone of excitation $\omega_R - \Omega$ (see Fig. 3) increases as Φ_C is increased above the minimum value given by Eq. (18). This latter variation is described by

$$(\omega_R-\Omega) = \{\ \Phi_C^2 (k_1^2/k_D^2)^2\ \Omega^2\ |M|^2 - \Gamma^2\ \}^{1/2} \quad . \tag{27}$$

(iii) The mode-mode coupling coefficient.

The mode coupling coefficient relates the normalized damping rate of the excited mode (Γ/Ω) to the pump mode amplitude necessary for coupling. A knowledge of such coefficients between various modes in the plasma may indicate how a multi-mode spectrum can develop. The coupling coefficient is in general complex, $M = M_r + i\ M_i$, and requires two separate experimental measurements for its complete determination. $|M|$ the absolute magnitude is measured from the variation of the minimum threshold Φ_M with the damped state of the excited mode Γ/Ω ; M_i/M_r the "argument" is determined by observing the phase α between the pump mode and the excited mode.

First, the magnitude of the coupling coefficient is obtained from

Eq. (18),

$$\frac{k_1^2}{k_D^2} |M| = - \frac{\Gamma/\Omega}{\Phi_M} \quad . \tag{28}$$

Γ/Ω , the ratio of the damping to the resonance frequency, and Φ_M , the minimum threshold amplitude, may be measured experimentally. Therefore, the magnitude of the coupling coefficient determined by the equation above may be compared to that evaluated for the parameters of the system by Eq. (14).

Secondly, the "argument" of the coupling coefficient is determined from the phase between the excited mode and the pump which may be derived from Eq. (5).[18] Assuming Φ_0 is real and $\Phi_1 = |\Phi_1| e^{i\alpha}$ in this equation, we solve for the phase angle α between the two modes, obtaining

$$\alpha = \frac{1}{2} \tan^{-1} \left\{ \frac{(M_i/M_r)[(\omega_0/2) - \Omega] + \Gamma}{(M_i/M_r)\,\Gamma - [(\omega_0/2) - \Omega]} \right\} \quad . \tag{29}$$

The variation of α with the frequency of the pump ω_0 is determined by M_i/M_r for experimentally measurable values of Γ and Ω . A typical variation of α for M_i/M_r computed from Eq. (14) for experimental parameters is given in Fig. 14. Thus a unique verification of the theoretical coupling coefficient M is possible with two complementary measurements.

Φ_0 in the expressions above is the amplitude of the pump mode externally excited in the stable plasma of the Q device. The temporal response of this plasma to external excitation of drift waves is quite similar to that associated with a harmonic oscillator subjected to an

external driver in both linear and nonlinear aspects.[17] Analogous to that of an oscillator, the steady state amplitude of a driven drift mode is dependent not only on the amplitude of the external driver but also on the frequency of excitation and on the damped state of the plasma. The steady state amplitude peaks approximately at the resonant frequency given by Eq. (9) and is inversely proportional to the damped state described by Eq. (10) for a given external excitation amplitude.

With this resonance variation of the externally excited pump mode, a comprehensive summary of the aspects of parametric coupling described above is schematically represented in Fig. 3. The lower abscissa gives the frequency of the pump mode; the upper abscissa gives that of the excited mode in accordance with Eq. (16). The ordinate specifies the amplitude of the pump Φ_0 . The inverse resonance curve bordering the shaded area representing Eq. (26) is the curve for the threshold as a function of $\omega_0/2 - \Omega$, the deviation from the optimum frequency. The vertical position of this curve depends on the damping of the excited mode Γ . Parametric excitation occurs with the intersection of the two curves (the enhancement of thermal fluctuations being ignored). Excitation cannot occur if the pump amplitude is too small or the damping of the excited mode is too high. As the pump amplitude is increased, coupling first occurs when the two curves intersect at one point (Φ_M, Ω) corresponding to the minimum threshold. As the pump amplitude is increased further, the two curves intersect at two points and the zone of excitation correspondingly increases. Parametric action is most intense near the center of the zone.

In the absence of dispersive corrections [C_Ω in Eq. (9)] the

resonance of the pump mode is exactly twice that of the excited mode (a). With dispersion the two modes are displaced. However, parametric excitation can still occur if the two curves overlap (b). For highly dispersive modes, excitation is not possible (c).

Above the minimum threshold parametric excitation is possible over a range of frequencies, Eq. (27). As the pump frequency is swept through this range, the phase between the two modes changes. As the pump frequency is increased, the excited mode initially leads and then lags behind the pump as described by Eq. (29) for experimental values of the parameters.

E. Saturation of the Excited Mode

In our steady state experiments, modes of finite amplitude are observed. Although growth rates resulting from the application of the pump have been calculated, we must in the final analysis include the amplitude limiting mechanisms which produce the observed steady state behavior. These mechanisms may be described in terms of a nonlinear damping factor Γ^{NL} which is related to the linear damping by

$$\Gamma^{NL} = \Gamma(1 + R\Phi_1^2) \quad . \tag{30}$$

Φ_1 is the amplitude of the excited mode. R is a proportionality factor discussed below. For simplicity, we have neglected the effect of the pump amplitude. We observe that this nonlinear damping of a stable mode Γ^{NL} is dependent on mode amplitude, damping increasing as the amplitude increases. This variation has been observed experimentally for externally driven stable drift modes.[17]

Physically, this variation of the damping rate with mode amplitude $\Gamma(1 + R\Phi_1^2)$ arises from several mechanisms. One possible mechanism is the depression of the density gradient produced by drift wave induced diffusion.[5] This change is described by the decrease in κ which varies as the square of the wave amplitude,[17] i.e., $\kappa^{NL} = \kappa - \Delta\kappa(\Phi_1^2)$. Examination of Eq. (10) written in the form below shows that this decrease in κ results in an increase of the damping rate for a stable plasma,

$$\Gamma^{NL} \simeq -\left\{\sigma - \frac{[k_y(V_i^2/\omega_{ci})\kappa^{NL}]^2 (k_y\rho_i)^2}{d_e^{NL}} [2 - 10(k_y\rho_i)^2 - 8(d_i^{NL}/d_e^{NL})] - 2\, d_i^{NL}\right\}$$

Another mechanism which can lead to nonlinear damping is wave-particle scattering suggested by Dupree.[11] From a kinetic analysis, Dupree finds that the basic effects of incoherent wave-particle scattering is the increase of the particle diffusion described in Sec. IIB. Specifically, electron diffusion is increased above that along $\underset{\sim}{B}$ associated with electron-ion collisions, $d_e^{NL} = (k_z^2 V_e^2/\nu_{ei}) + d_e^{W}(\Phi_1^2)$, and ion diffusion transverse to $\underset{\sim}{B}$ is increased beyond that resulting from ion-ion collisions, $d_i^{NL} = [\frac{1}{4}(k_y\rho_i)^4 \nu_{ii}] + d_i^{W}(\Phi_1^2)$. Both additional diffusion fluxes vary as the square of the wave amplitude. These changes resulting from the increase in wave amplitude lead again to an increase of the damping rate, as observed in the equation above.

With the assumption that the nonlinear modifications from the two mechanisms described are small compared to the original linear terms, the nonlinear damping rate above takes the form given in Eq. (30).

R in this equation has been computed and found to be dependent primarily on the change in κ.[17]

The relation of the nonlinear damping Γ^{NL} to the steady state amplitude of the excited mode is observed by the substitution of Eq. (30) into Eq. (17), yielding

$$\gamma^{NL} = \Gamma(1 + R\Phi_1^2) + \{(\Phi_0^2/\Phi_M^2)\Gamma^2 - [(\omega_0/2) - \Omega]^2\}^{1/2}$$

which describes the nonlinear growth rate for the excited mode above threshold. Saturation in amplitude of this mode is related to the vanishing of γ^{NL}. For saturation at resonance $(\omega_0/2 = \Omega)$ we find

$$\Phi_{1S}^2 = (1/R)\{(\Phi_0/\Phi_M) - 1\} \tag{31}$$

which shows that, above the minimum threshold Φ_M, Φ_{1S}^2 varies linearly with the pump amplitude Φ_0. R of Eq. (30) is obtained from the reciprocal of the slope of this curve for an approximated value of Φ_M as shown in Sec. IVD.

III. EXPERIMENTAL ARRANGEMENT

The experiment was conducted in a highly ionized potassium plasma of a Q device,[8] Fig. 4. The plasma approximately 5.8 cm in diameter is generated by surface ionization of atomic beams on tungsten plates heated to above 2200°K by electron bombardment and by thermal emission of electrons from these plates. The atomic beam at each end of a 70 cm long column is collimated so that the density gradient maximum occurs inside the plasma, separating it from the temperature and potential gradient maxima occurring at the edge of the cylindrical plasma which coincides with the edges of the plates. Our investigation of parametric coupling is concerned mainly with drift waves occurring at the density gradient maximum although similar parametric processes also take place for waves occurring at the edge of the plasma.

The plasma and the plasma source are housed in an evacuated stainless steel cylinder 6 in. in diameter. The system is maintained at 10^{-6} Torr during operations. The plasma is collimated by a uniform axial magnetic field (0 to 4.5 kG) produced by a water-cooled solenoid. Probes measuring various plasma parameters are inserted through any of 12 ports along the cylindrical shell. Axial variations are measured by probes entering through the end flange on which the plasma source is mounted. Radial density and potential measurements are facilitated by the use of mechanized probes coupled to a X-Y recorder.

Density gradient drift waves are detected by shielded Langmuir probes, biased negatively to measure density fluctuations or floated to measure potential fluctuations, as shown in Fig. 5. Fluctuations are

identified as density gradient driven drift waves by the following criteria: (1) The oscillations are detected at the density gradient maximum inside the plasma rather than at the edge where the potential and temperature gradients achieve their maxima. (2) The direction of propagation of the waves is in the electron diamagnetic direction. In addition to the direction of propagation, the mode numbers of the waves are determined by noting the phase relation between signals received by 3 probes displaced azimuthally by 90 degrees from one another. For an externally driven mode, a signal with the gated waveform shown in Fig. 6 may be used for positive determination of the direction and mode of azimuthal propagation. (3) Drift waves are low frequency waves, 1 to 10 kHz, for the Q device described. The waves show the proper frequency and damping variations with magnetic field and density.[15] The waves exhibit a mode structure described by the linear dispersion relation.[13],[15]

Drift waves in a stable plasma are excited by modulating the potential of a tungsten grid,[9] 1 cm square with mesh 50 lines/in. The grid, mounted on a radial probe and placed at the density gradient maximum, has its plane parallel to the axis of the plasma, Fig. 5. Drift waves can be excited with either a floating grid or a grid biased at or below the plasma potential. However, to minimize the extraneous efforts of d-c currents, the excitation signal is usually capacitatively coupled to the plasma.

To excite a specific mode and to couple most effectively to the plasma, the external oscillator is tuned to the peak resonance of the mode. At resonance, the amplitude of the excited wave increases as the

amplitude of the driving signal is increased until saturation occurs.

Temporal damping associated with a particular drift mode in a stable plasma may be directly measured because of the periodicity of the mode in the azimuthal direction. An external signal at the resonant frequency is applied to the excitation grid through a gated tone burst generator, Fig. 5. The latter device modulates the signal in the manner shown in the top trace of Fig. 6. The behavior of the drift wave excited in the plasma as detected by a Langmuir probe is shown in the lower trace. The wave observed grows, reaches steady state, and then decays. Measurement of the decaying portion of the wave gives the damping rate of the mode being excited.

Drift wave characteristics (e.g., frequency and damping) are dependent on the parameters of the system such as density, density gradient, potential, magnetic field, and plasma temperature. The density, the density gradient and the plasma potential are determined easily with shielded Langmuir probes. The magnetic field is measured with a gaussmeter (Bell-Model 240) capable of better than 3% accuracy. The temperature of the ionizing plates which is assumed for that of the electrons and the ions is measured with an optical pyrometer (Pyro-No. 95). Drift wave frequencies, spectra, and amplitudes are accurately determined by either a spectrum analyzer (Singer-metrics-Model SPA3) or a wave analyzer (General Radio-Type 1900A). The temporal and phase characteristics of drift waves are investigated easily with a dual beam oscilloscope (Tektronix-Type 555).

IV. EXPERIMENTAL RESULTS

The experimental results given in this section describe principally the degenerate case of three-mode parametric coupling in which the two excited modes are identical. To effect parametric excitation of a stable drift mode near the $m = 1$ resonant frequency Ω, a pump mode is externally excited at the frequency $\omega_0 \simeq 2\Omega$, corresponding to the $m = 2$ mode. Various aspects of this process are examined in Secs. IVA-IVD.

A brief examination of nondegenerate and higher mode coupling schemes observed experimentally is given in Sec. IVE. Although these more complex schemes may be observed with density gradient drift waves, they are more readily observable with temperature gradient drift waves occurring near the edge of the cylindrical plasma. In Sec. IVF, observation of degenerate three-mode parametric coupling in the unstable regime is presented and discussed.

A. Observation of Parametric Coupling

For degenerate three-mode parametric coupling of drift modes in a stable plasma, four primary conditions must be met. First, the external signal must couple effectively to the plasma so as to be able to drive the pump mode to sufficiently large amplitudes. Therefore, the pump mode is driven near the $m = 2$ resonance $\omega_0 \simeq \Omega$ $(m = 2)$ with the damping associated with this mode being relatively small. Secondly, the damping associated with the excited mode Γ must also be small so as to allow a small threshold amplitude Φ_C, Eq. (26). Next, wave numbers

must be conserved, $k_0 = 2k_1$ $(k = m/r_0)$, which is not a problem because of m being an integer and r_0 being approximately the same for both modes. Finally, frequencies must be matched, $\Omega(m=2) \simeq 2\Omega(m=1)$. Parametric coupling is not possible with highly dispersive modes as discussed in Sec. IID. Experimental data supporting these assertions are given and discussed below.

The radial positions of both the pump and the excited mode together with the radial profiles of the density and the plasma potential are given in Fig. 7. The density profile shows that at the localized radial positions of the waves, the assumption $-\frac{1}{n}\frac{\partial n}{\partial x} = \text{constant}$ in Sec. IIA is a valid approximation. The potential profile shows the presence of a radial electric field which would contribute to the frequency observed in the laboratory frame.

Parametric coupling occurs for a range of experimental conditions. The local density at the wave maximum ($1.5\ \text{cm} < r_0 < 2.0\ \text{cm}$) ranges from $7 \times 10^9\ \text{cm}^{-3}$ to $5 \times 10^{10}\ \text{cm}^{-3}$. The normalized density gradient varies from .7 to 1.0. The radial electric field varies from .1 V/cm to .25 V/cm. The range of the magnetic field is .6 kG to 1.0 kG. For these ranges of experimental parameters, the observed frequency of the parametrically excited mode ranges from $\sim$ 2 kHz to $\sim$ 6 kHz. Under these conditions, the approximations assumed in Sec. IIA, $\omega/\omega_{ci} \simeq .1 \ll 1$, $k_y\rho_i \simeq .2 \ll 1$, are still valid.

Examination of Fig. 7 shows that the positions of the peaks of the two coupled modes are close together (< 5 mm). The profiles show that the excited mode is more localized than the pump mode. The dispersal of the pump mode is caused probably by the relatively large size of the

exitation grid and the finite extent of the exciting field. The parametrically excited mode is concentrated radially because its amplitude, like that of an unstable mode, depends primarily on the spatial distribution of the growth parameters, e.g., the density gradient.

The direction of propagation and the mode number of the excited mode and those of the pump mode are determined in the manner described in Sec. III with the appropriate band-pass filtering. The pump mode at frequency ω_0 is identified as a $m = 2$ mode propagating in the electron diamagnetic drift direction. The excited mode is identified as a $m = 1$ mode propagating also in this direction, in agreement with theory.

The frequency of the excited mode is half that of the pump mode to within 10 Hz (measured with the wave analyzer), in agreement with Eq. (16) which predicts $\omega_R = \omega_0/2$. This ratio of frequencies has occurred for all the cases of degenerate mode coupling investigated. The frequency of the excited mode and that of the pump mode agree with the frequency of the $m = 1$ resonance and that of the $m = 2$ resonance, respectively, to within 10%. The frequency and damping of both resonant drift modes have been measured and are in agreement with the predictions of linear theory.[15]

The spectrum of the parametrically excited mode is easily observed with either the spectrum analyzer or the wave analyzer. However, for a continuous measurement of the variation of the peak amplitudes of the two coupled modes with the amplitude of the external excitation, the wave analyzer and an oscillator are applied in the following manner. The pump mode is excited by the oscillator whose output amplitude is placed on the X axis of a recorder. The excited modes detected by a

Langmuir probe are fed into the wave analyzer locked, first, to the pump frequency and then to the excited mode frequency. This input to the analyzer is recorded on the Y axis. Thus, the wave amplitudes of both modes as continuous functions of the external oscillator strength are recorded. Finally, a calibration of voltage output versus power delivered by the oscillator is obtained to examine the distribution of power between the two coupled modes.

The steady state data obtained by this method reveal that as the amplitude of the external signal at ω_0 is increased, the amplitude of the pump mode first emerges above the thermal noise level. Accompanying this increase in amplitude of this mode is the enhancement of the thermal fluctuation spectrum near $\omega_0/2$. Then as the pump mode reaches the threshold for coupling, the excited mode at $\omega_0/2$ increases rapidly and becomes coherent. Above threshold, the amplitudes of both modes increase further and eventually saturate with increase of the external signal.

Following the procedure used in Sec. II, for analysis we divide this experimental process into three regimes--below threshold, at threshold, and above threshold--which are individually examined in the following sections.

B. Behavior of the Fluctuation Spectrum

To observe the enhancement of the fluctuation spectrum below threshold, a description of the excited mode at $\omega_R = \omega_0/2$ is obtained with the wave analyzer. Representative power spectra (power is assumed to be proportional to Φ_1^2) derived from these analyzer data for the

excited mode are given in Fig. 8. The line shape observed for several values of pump amplitude is compared with that predicted by Eq. (22) for an equilibrium situation ($f = 1$). The asymmetry observed in the data may be due to the nonequilibrium condition (the density gradient) occurring experimentally. The values of Γ/ω_R, the ratio of damping to frequency, and Φ_0/Φ_M, the ratio of pump amplitude to minimum threshold amplitude, used in Eq. (22) are those measured experimentally for this set of data. Φ_M is determined by the method described in the next section.

The variation of the normalized peak spectral density $S(\Omega)$ below threshold as a function of the pump amplitude normalized to the threshold is given in Fig. 9. The results showing the rise of the excited mode with the pump are well described theoretically by Eq. (23) where $\Phi_M = .04$ is assumed for the experimental normalization factor. Near threshold where the spectrum of the excited mode can be measured accurately, we have observed a similar, though less rapid, rise in the integrated spectrum according to the description of Eq. (24).

The balance of power between the external source and the two coupled modes is examined in Fig. 10. The self-consistent pump power P_0 (proportional to Φ_0^2) and the peak fluctuating excited mode power P_1 (proportional to Φ_1^2) are plotted as functions of the power input P_{EX} in Fig. 10. We observe that P_0 departs from a linear variation just as P_1 begins to rise, a change predicted by Eq. (25). The sum of the power dissipated by the two modes, taking into account the total integrated power about ω_R (obtained from spectra such as those shown in Fig. 8) and the relative damping of the two modes, Γ and Γ_0

(measured directly), varies linearly with P_{EX} in agreement with that described by Eq. (25). This variation is represented by the Σ line in Fig. 10.

C. Determination of the Threshold and the Coupling Coefficient

Theoretically, the threshold may be defined as the pump amplitude at which the rate of increase of the peak power density is a maximum, by Eq. (23) and Fig. 9. Correspondingly, the experimental threshold is defined as the minimum value of the pump amplitude at which the excited mode is observed to rise most rapidly. This threshold usually corresponds to the instance at which the excited mode is first distinctly and steadily observed above the thermal noise as the pump amplitude is increased. Therefore, this threshold is determined either visually by a sequence of spectra obtained with a spectrum analyzer or with a wave analyzer plot described in Sec. IVA.

Threshold for excitation is observed to vary with change in the parameters of the system and to be related particularly to the damping of the excited mode. Figure 11 gives experimental data relating the minimum threshold and the damping. The threshold is measured in terms of either the fluctuating potential or the fluctuating density ($\Phi_0 = n_1/n_0$) . The damping is determined by the method described in Sec. III. The results show approximately a linear variation and agree with Eq. (18) which states that the threshold must increase with increase of the damping rate of the excited mode. The magnitude of the coupling coefficient $k_1^2/k_D^2\ |M|$ obtained from the inverse slope is $0.7 \pm .2$. The theoretical value based on the experimental parameters

and calculated from Eq. (14) is $\sim .25$. This agreement between the two values is acceptable considering the approximations used in deriving the theoretical value. The spread in the experimental data may be related to the change in the coupling coefficient as Γ is varied.

The threshold as defined above and as observed experimentally is consistent with that used to obtain the best fit of the enhancement of the fluctuation spectrum $S(\omega_1)$, the peak of the spectrum $S(\Omega)$, and the integrated spectrum $\int S(\omega_1)\, d\omega_1$.

Threshold at minimum pump amplitude is possible at only one value of frequency. However, if the pump amplitude is increased, parametric excitation can occur over a band of frequencies in agreement with the predictions of Eq. (27). The width of the band increases with increase in pump amplitude. Experimental data showing this variation are given in Fig. 12. The results follow closely those predicted by Eq. (27) for the experimentally observed parameters.

Below threshold, the phase of the excited mode relative to that of the pump mode cannot be determined. Above threshold the waves become coherent. A scope trace of the two waves occurring simultaneously above threshold is shown in Fig. 13. Through Fourier analysis or direct simulation, the relative phase between the two modes may be deduced. Simulation of the waveform in Fig. 13 is easily achieved by superposition of a wave at ω_R and a wave at $\omega_0 = 2\omega_R$ by means of a frequency doubler circuit with a variable phase delay. Calibration of the delay yields the relative phase immediately. Decomposition of the waveform in Fig. 13 as the sum of $|\Phi_0| \cos(2\omega_R t)$ and $|\Phi_1| \cos(\omega_R t + \alpha)$, where $|\Phi_0|$ and $|\Phi_1|$ are the amplitudes, gives $\alpha \simeq 0$.

Above the minimum threshold, excitation occurs over a range of frequencies. As the frequency of the pump is swept through this range, the relative phase between the pump and the excited mode changes. A typical phase variation observed experimentally is shown in Fig. 14. As the frequency is increased, the excited mode leads the pump at onset of parametric coupling but lags at the cutoff. This variation agrees with that predicted by Eq. (29) evaluated with the observed parameters of the system. Although Eq. (29) was derived essentially from a linear theory and the phase observed is associated with steady state, finite amplitude drift modes (a nonlinear aspect), the agreement between the two is significant.

With the magnitude determined by the threshold measurement shown in Fig. 11 and the argument determined by the phase measurement shown in Fig. 14, the complex coupling coefficient is experimentally resolved and agrees qualitatively with that obtained theoretically, Eq. (14).

D. Steady State Amplitude of the Coupled Modes

Above threshold, the steady state, saturated amplitude of both modes increases with increase in external excitation. Both mode amplitudes are limited at large external signals. First, variation of the pump amplitude is considered. In the linear regime below threshold, the pump amplitude is determined by the amplitude of the steady state external signal and by the damped state of the system; the pump frequency is assumed to be near the $m = 2$ resonance. As the external excitation is increased, the pump mode increases in amplitude, excites the mode near the $m = 1$ resonance, and eventually reaches a limited

value. Limitation of this pump mode occurs for the following reasons: (1) Coupling of large excitation signals to the plasma by a metallic grid is ineffective because of sheath effects. (2) The nonlinear mechanisms of change in the density gradient and wave-particle scattering produce an increased damped state of the system. (3) Energy is transferred from the pump mode to the excited mode in the parametric excitation process.

Limitation in the amplitude of the excited mode occurs in two ways: (1) At a particular value of pump amplitude corresponding to a definite value of external excitation, the steady state, saturated amplitude of this mode is observed. This saturation we have assumed results from the nonlinear mechanisms of change in the density gradient and wave particle scattering as discussed in Sec. IIE. (2) This saturated amplitude of the excited mode is limited with respect to increase in external signal. This latter restriction results from limited amplitude of the pump mode and from the nonlinear mechanisms mentioned above.

An examination of the steady state amplitude of the excited mode as a function of the pump amplitude obtained from a wave analyzer plot is given in Fig. 15. Neglecting the region of enhanced thermal fluctuations in the data, we observe that Φ_{1S}^2 varies linearly with pump amplitude Φ_0 in agreement with the variation predicted by Eq. (31). Extrapolation of the data above threshold yields $\Phi_M = 3.5 \times 10^{-2}$. With this approximation for Φ_M, R, a measure of the strength of the nonlinear damping mechanisms discussed in Sec. IIE, in Eq. (31) obtained from Fig. 15 is ~ 17. The theoretical value for R based on the expression used in the study of nonlinear damping of a single mode[17]

and computed for the experimental conditions encountered in parametric coupling is ~ 40. The discrepancy between the experimental and the theoretical values may be partially due to the neglect of the pump mode in the description of nonlinear damping.

E. Nondegenerate and Higher Mode Coupling Schemes

Parametric coupling of the $m = 1$ and the $m = 2$ mode by a $m = 3$ pump mode has been observed for density gradient drift waves under the conditions of a relatively high thermal fluctuation spectrum and of very broad resonances for the modes involved. Coupling of all three lower modes by a $m = 4$ pump mode has also been observed under these particular conditions.

These complex coupling schemes may be observed under less stringent conditions with temperature gradient drift waves occurring at the edge of the plasma. Here, the temperature gradient as well as the potential gradient reach their maxima, Fig. 7. Drift waves observed in this region usually exhibit higher frequencies than those occurring inside the plasma.

Spectra describing nondegenerate parametric coupling with temperature gradient drift waves are given in Fig. 16. The thermal fluctuation spectrum in this region shows that all the modes involved are lightly damped which facilitates the driving of the pump mode above threshold and the parametric excitation of the coupled modes. In addition, the fluctuating mode frequencies are near multiples of the fundamental which satisfies the frequency matching conditions required for coupling. Although these coupling processes may be easily observed, they may be

difficult to describe theoretically, being at the edge of the plasma where large, sheared electric fields must be considered in addition to the large temperature gradient. Except for a qualitative examination, we have not investigated parametric coupling with this set of drift waves.

F. Parametric Coupling in an Unstable Plasma

In the preceding sections, we have examined parametric coupling only in a stable plasma in which the pump mode was externally excited. In this section, we relate observations which suggest parametric coupling in the unstable regime in the absence of external excitation. The case observed is the degenerate three-mode coupling shown in Fig. 17. As the magnetic field is increased from 1.95 kG to 2.35 kG (the top three traces) the $m = 4$ drift mode first goes unstable, and as its amplitude increases it excites the $m = 2$ mode at frequency $\omega_1 = \omega_0/2$, exactly half the frequency of the $m = 4$ mode. With further increase in the magnetic field, both modes increase and then decrease in amplitude. Beyond this range of magnetic field, other modes appear, due to the change in the mode stability condition with field (the bottom trace). Observation of the two coupled modes, ω_0 and ω_1, on the oscilloscope reveals a phase variation similar to that described in Sec. IVC in which the excited mode leads and then lags behind the pump mode as the latter mode increases in frequency.

This variation of the two coupled modes in Fig. 17 describes a naturally occurring parametric coupling process and not just the simultaneous occurrence of the $m = 2$ and $m = 4$ modes because the

frequencies of the two modes are integrally related ($\omega_0 = 2\omega_1$) through the entire range of coupling. This relationship does not occur for unstable drift modes described by linear theory because of corrections arising from finite Larmor radius and other effects, Eq. (9), which results in $\omega_0(m=4) \neq 2\omega_1(m=2)$. The assertion above is further justified by the similarity of the phase variation observed between the two modes in Fig. 17 to that observed in the case of parametric coupling in a stable plasma.

From the sequence of spectra shown in Fig. 17, it appears that coupling could serve as an amplitude limiting mechanism for the unstable (pump) mode because the energy available is now distributed over two or more modes. Furthermore, parametric coupling could be the mechanism producing a multi-mode spectrum in which the high frequency mode first appears and then the low frequency modes, all modes satisfying the frequency and wave number matching conditions.

V. CONCLUSION

Parametric coupling between resonant drift modes in the collisional plasma of a Q device has been clearly identified through examination of the various aspects described in this paper. More specifically, the functional behavior of the degenerate case of three-mode parametric coupling has been investigated extensively and found to vary in the manner described by theory. Below threshold, the thermal fluctuation spectrum is enhanced by the coupling process. At threshold, parametric excitation is dependent not only on the damping associated with the excited mode and on the pump amplitude but also on the frequency of the pump. The experimental and theoretical thresholds obtained agree to within the approximations assumed.

Enhanced diffusion of the plasma which manifests itself in the decrease of the density gradient has been shown to occur with drift waves[13],[17] and to lead to nonlinear damping associated with a drift mode.[17] Therefore the assumption of this phenomenon as one of the primary mechanisms limiting the amplitude of the excited mode is valid and yields a model describing the observed variation.

Externally initiated nondegenerate and higher order mode coupling schemes have been observed and could have been investigated by the methods used in this paper. Moreover, these methods may be applicable to other parametric schemes in plasmas or to parametric processes in other types of systems. Of particular significance, parametric coupling in an unstable plasma has been identified through comparison of the behavior of the modes with that observed in the case of externally

induced parametric coupling in a stable plasma.

ACKNOWLEDGMENTS

The authors are indebted to R. Rowberg for his useful suggestions and able experimental assistance. The enlightening discussions with G. Weyl and M. V. Goldman are gratefully acknowledged. The technical assistance of Z. Lucky has been invaluable.

REFERENCES

1. R. A. Stern and N. Tzoar, Phys. Rev. Letters 17, 903 (1966);
C. W. Mendel and R. A. Stern, Bull. Am. Phys. Soc. 13, 304 (1968);
D. W. Ignat and J. L. Hirshfield, Bull. Am. Phys. Soc. 13, 304 (1968);
S. Hiroe and H. Ikegami, Phys. Rev. Letters 19, 1414 (1967);
M. Yoseli, J. Phys. Soc. Japan 23, 611 (1967);
J. H. Krenz and G. S. Kino, J. Appl. Phys. 36, 2387 (1965).

2. V. P. Silin, Zh. Eksperim. i Teor. Fiz. 47, 1977 (1965;
English transl.: Soviet Phys.-JETP 21, 1127 (1965).

3. D. F. DuBois and M. V. Goldman, Phys. Rev. Letters 14, 544 (1965);
Phys. Rev. 164, No. 1, 207 (1967); Phys. Rev. Letters 19, 1105 (1967);
Y. C. Lee and C. H. Su, Phys. Rev. 152, 129 (1967);
E. A. Jackson, Phys. Rev. 153, 235 (1967);
K. Nishikawa, J. Phys. Soc. Japan 24, 1152 (1968).

4. D. Montgomery and I. Alexeff, Phys. Fluids 9, 1362 (1966);
D. Montgomery and R. C. Harding, Phys. Letters 23, 670 (1966);
M. Yosell, J. Phys. Soc. Japan 23, 1150 (1967).

5. A. Y. Wong, F. Hai and R. Rowberg, Paper B-6, International Symposium on Fluctuation and Diffusion in Plasmas, Princeton University, June 1967;
F. Hai, R. Rowberg, and A. Y. Wong, Bull. Am. Phys. Soc. 13, 305 (1968).

6. G. Weyl and M. Goldman, University of California, Los Angeles, Plasma Physics Group Report No. R-32, May 1968.

7. T. H. Stix, Princeton Plasma Physics Laboratory, Princeton University Report No. Matt-588, 1968.

8. N. Rynn and N. D'Angelo, Rev. Sci. Instr. 31, 1326 (1960).

9. A. Y. Wong and R. Rowberg, Phys. Rev. Letters 18, 390 (1967).

10. A. Y. Wong, M. V. Goldman, F. Hai, and R. Rowberg, Phys. Rev. Letters 21, 518 (1968).

11. T. H. Dupree, Dept. of Nuclear Engineering and Research Laboratory of Electronics Report, Massachusetts Institute of Technology 1968.

12. F. W. Perkins, T. K. Chu, B. Coppi and H. W. Hendel [Bull. Am. Phys. Soc. 13, 1947 (1968)] have reported that the results from a rectangular coordinate treatment are descriptive of drift modes occurring in a cylindrical system.

13. H. W. Hendel, B. Coppi, F. Perkins and P. A. Politzer, Phys. Rev. Letters 18, 439 (1967);
H. W. Hendel, T. K. Chu and P. A. Politzer, Phys. Fluids 11, 2426 (1968).

14. The contributions to coupling coming from the convective term in the ion equation of motion was shown by Weyl and Goldman to be negligible. In addition, they have considered coupling terms in the collision-free part of the ion-fluid stress tensor which have been omitted here for simplicity.

15. R. Rowberg and A. Y. Wong, University of California, Los Angeles, Plasma Physics Group Report No. R-39, Feb. 1969.

16. G. Bekefi, Radiation Processes in Plasmas (John Wiley and Sons, Inc., New York, 1966). See Chapter 4.

17. F. Hai and A. Y. Wong, University of California, Los Angeles, Plasma Physics Group Report No. R-41, Feb. 1969.

18. This analysis is similar to that of R. Goldman (Technical Note BN-521, University of Maryland, Dec. 1967).

LIST OF FIGURES

Figure

1. Schematic of three-mode parametric coupling. The solid arrows represent interacting modes, the pump at ω_0 and the fluctuating modes at ω_1 and ω_2, which satisfy the frequency matching condition. The dashed arrows indicate feedback at $(\omega_0-\omega_2) = \omega_1$ and $(\omega_0-\omega_1) = \omega_2$ stemming from mode-mode coupling which leads to the enhancement of the fluctuating modes at ω_1 and ω_2, respectively.

2. Flow of energy in the parametric process. In the nonlinear regime, the damping associated with each of the two modes (Γ,Γ_0) depends also on the mode amplitudes (Φ_1,Φ_0).

3. Schematic of the conditions required for degenerate three-mode parametric coupling. The upper and lower abscissas follow the frequency relation given by Eq. (16). The ordinate indicates the amplitude of the pump. Φ_C represents the threshold for coupling. Curves a, b, and c represent pump amplitudes associated with constant external excitation levels as the pump frequency is varied. Curve a -- the pump resonance is exactly twice the excited mode resonance, $\Omega_0(m=2) = 2\Omega(m=1)$. Curve b -- although $\Omega_0 \neq 2\Omega$ because of dispersive effects, coupling is still possible. Curve c -- the resonant frequencies are so mismatched that coupling cannot occur.

Figure

4. Schematic of the Q device producing a highly ionized plasma. (A) plasma; (B) tungsten plate; (C) filaments; (D) oven; (E) solenoid; (F) pump; (G) axial probe; (H) radial excitation probe; (I) radial Langmuir probe.

5. Schematic for excitation and detection of drift waves. The signal from the tone burst generator is gated for damping measurements and direct for steady state excitation. The signal picked up by the detection probe is direct for potential measurements and biased for density measurements.

6. A typical oscillogram observed in the determination of the damping rate. Top trace -- signal on the excitation grid (5 V/cm); lower trace -- amplified signal from a Langmuir probe (5 mV/cm); time (1 ms/cm).

7. Radial profiles. The data are for a potassium plasma. B = 770 G, T = 2200 K, and axial column length - 70 cm. The frequencies of the excited mode and the pump are 5.16 kHz and 10.32 kHz, respectively.

8. Representative power spectra illustrating the enhancement of the fluctuation spectrum about 5.42 kHz as the pump power at 10.84 kHz is increased. The theoretical curves are obtained from Eq. (22) with the experimentally observed values of Φ_0/Φ_M and $\Gamma/\Omega = 2.9 \times 10^{-2}$.

Figure

9. Peak spectral density $S(\Omega)$ below threshold normalized to the spectral density without coupling $S_{M=0}(\Omega)$ as a function of the normalized pump mode amplitude Φ_0/Φ_M. The theoretical curve is obtained from Eq. (23). The data are for $n_0 = 1.5 \times 10^{10}$ cm^{-3}, T = 2200 K, B = 660 G, and axial column length = 70 cm.

10. Peak spectral density P_1 at ω_1 and the self-consistent pump power P_0 at ω_0 as functions of the oscillator power P_{EX}. Σ represents the total power dissipated at ω_1 and ω_0 obtained by computing the r.h.s. of Eq. (25), taking into account the total enhanced spectrum about ω_1.

11. The magnitude of the coupling coefficient determined by the normalized pump threshold Φ_M as a function of the damping rate of the excited mode. The different symbols represent different runs. The coupling coefficient $k_1^2/k_D^2\,|M|$ is given by the inverse slope of the line best fitted to the data. The ranges of the experimental parameters are 7×10^9 cm$^{-3} < n_0 < 2 \times 10^{10}$ cm^{-3} and 650 G < B < 800 G. The theoretical line is from Eq. (14) for mean values of the parameters in this range.

12. The threshold dependence on the pump frequency. The theoretical curve is from Eq. (27) with the experimentally measured values of the damping rate and the coupling coefficient.

Figure

13. Oscillogram of the parametric process above threshold. Top trace -- signal on the excitation grid (2 V/cm); lower trace -- amplified signal from a Langmuir probe (5 mV/cm); time (.1 ms/cm).

14. Variation of the phase between the pump and the excited mode as the pump frequency is varied. The theoretical curve is obtained from Eq. (29) with M_i and M_r computed from Eq. (14) and Γ/Ω measured experimentally.

15. Peak spectral density Φ_1^2 above threshold as a function of the pump amplitude Φ_0. The theoretical line obtained from Eq. (31) and fitted to the data above threshold gives $R \simeq 17$.

16. Spectra showing nondegenerate parametric coupling with temperature gradient drift waves. The externally excited mode at ω_0 is the pump and those at ω_1, ω_2, and ω_3 are the excited modes.

17. Spectra showing the occurrence of degenerate three-mode parametric coupling in an unstable plasma as the magnetic field is increased. The density gradient drift mode at ω_0 is the self-excited pump and that at ω_1 is the parametrically excited mode. The peak at the extreme left is the zero frequency marker.

FREQUENCY MATCHING CONDITION

$$\omega_0 = \omega_1 + \omega_2$$

ω_0 - PUMP MODE

ω_1, ω_2 } - FLUCTUATING MODES

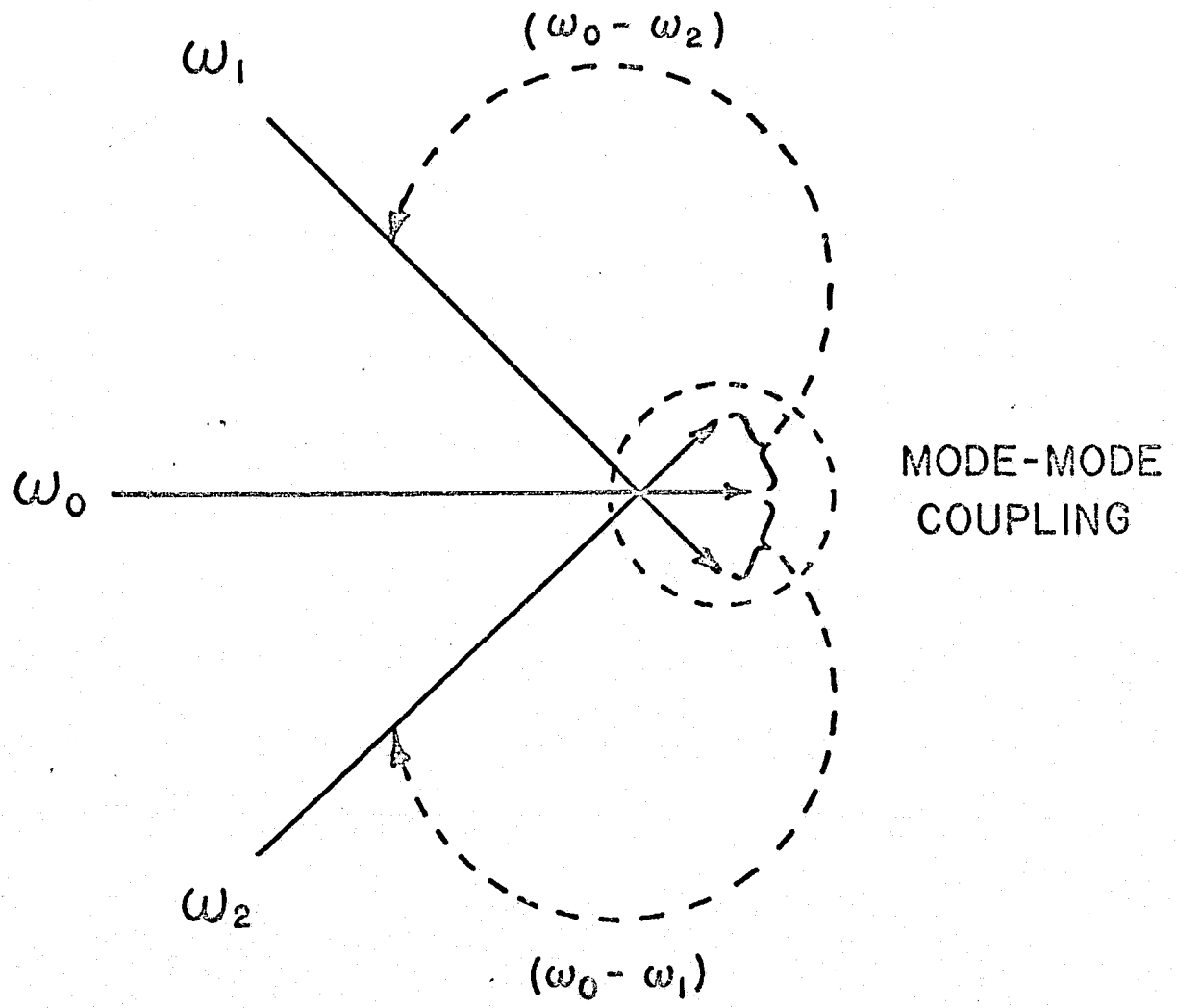

FIG. 1

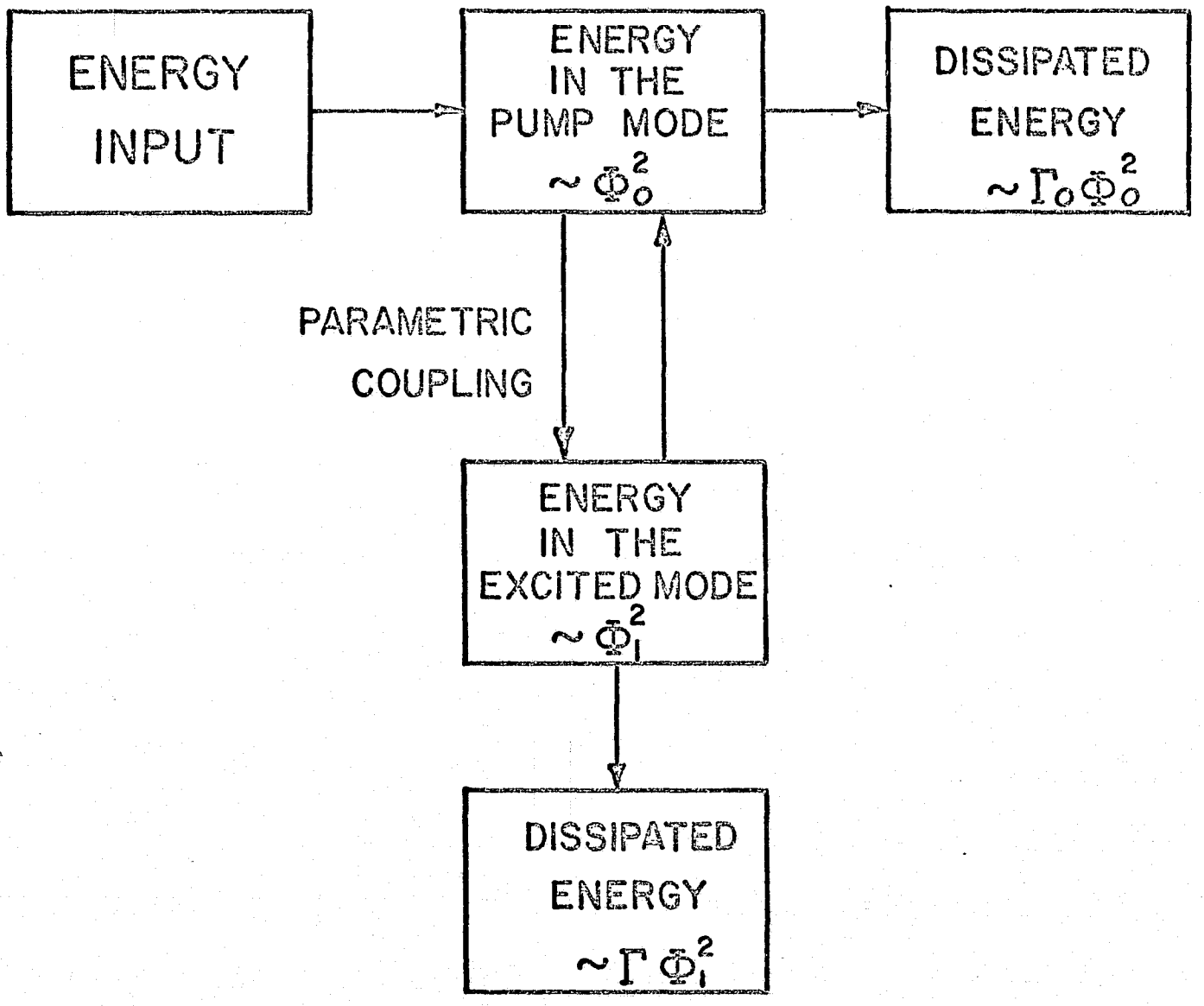
ENERGY INPUT
ENERGY IN THE PUMP MODE
$\sim \Phi_0^2$
DISSIPATED ENERGY
$\sim \Gamma_0 \Phi_0^2$
PARAMETRIC COUPLING
ENERGY IN THE EXCITED MODE
$\sim \Phi_1^2$
DISSIPATED ENERGY
$\sim \Gamma \Phi_1^2$

FIG. 2

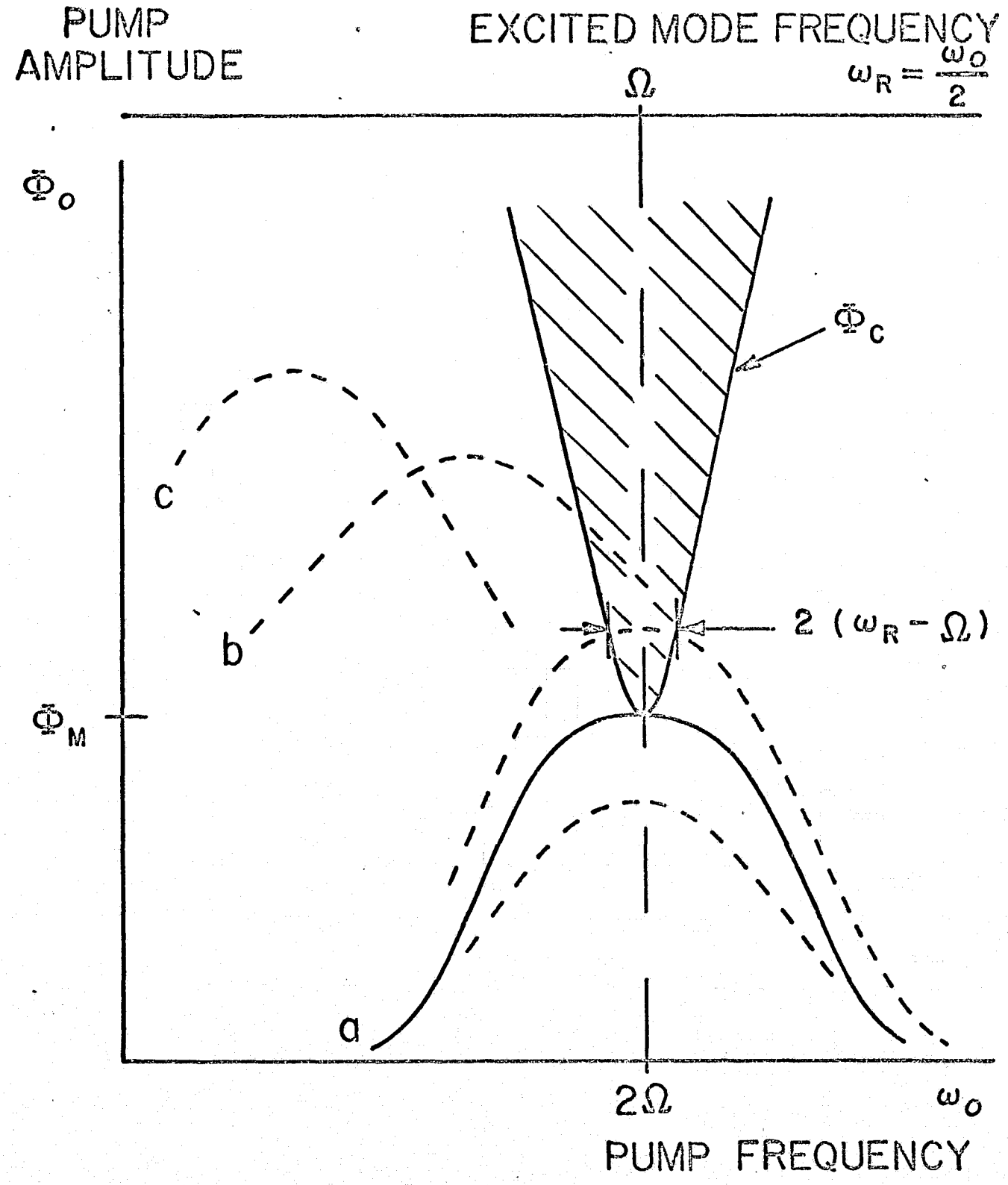
PUMP
AMPLITUDE
EXCITED MODE FREQUENCY
$\omega_R = \frac{\omega_o}{2}$
Ω
Φ_o
Φ_c
c
b
$2(\omega_R - \Omega)$
Φ_M
a
2Ω
ω_o
PUMP FREQUENCY

FIG. 3

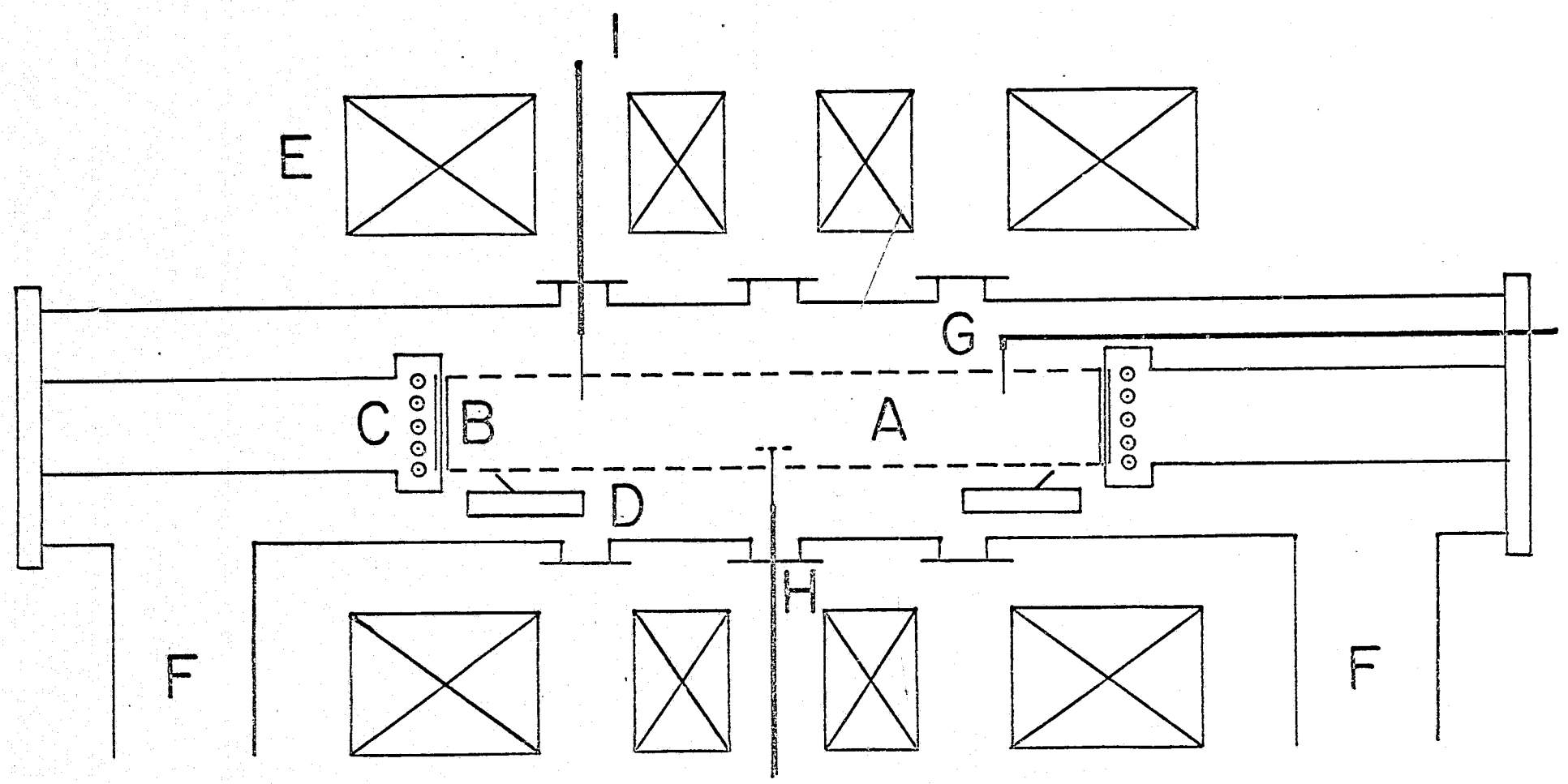

FIG. 4

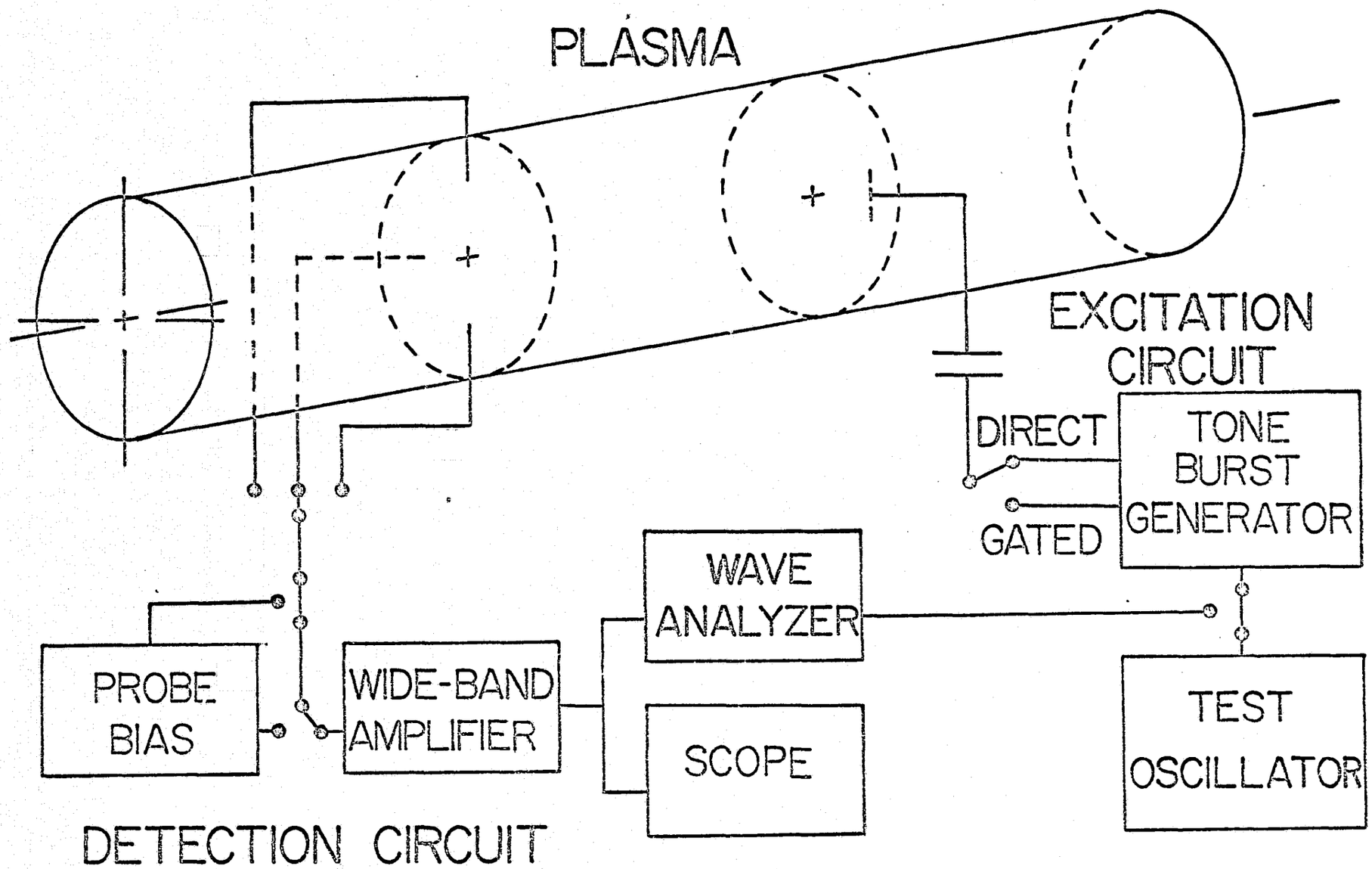
PLASMA
EXCITATION
CIRCUIT
DIRECT
GATED
TONE
BURST
GENERATOR
WAVE
ANALYZER
SCOPE
TEST
OSCILLATOR
PROBE
BIAS
WIDE-BAND
AMPLIFIER
DETECTION CIRCUIT

Fig. 5

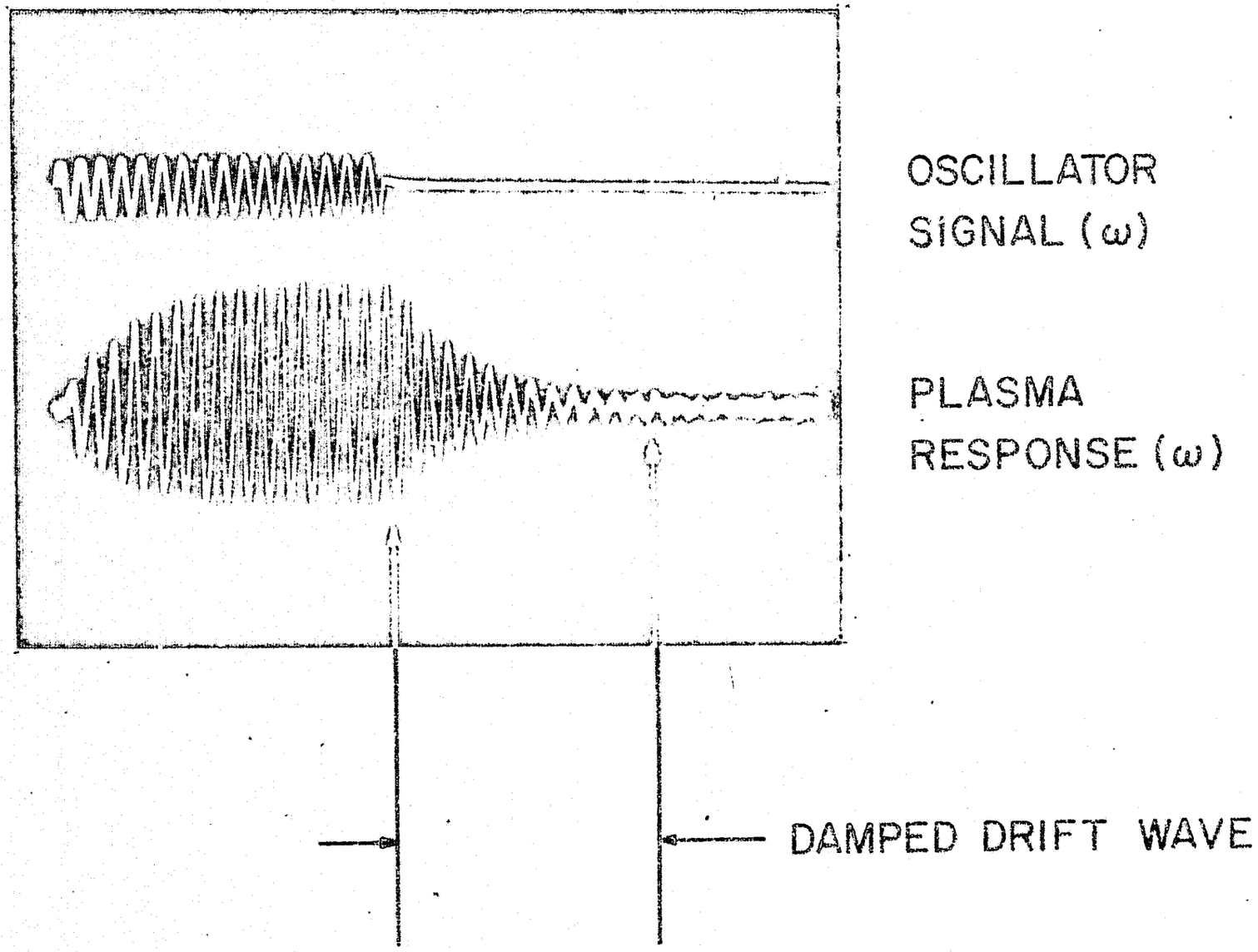

FIG. 6

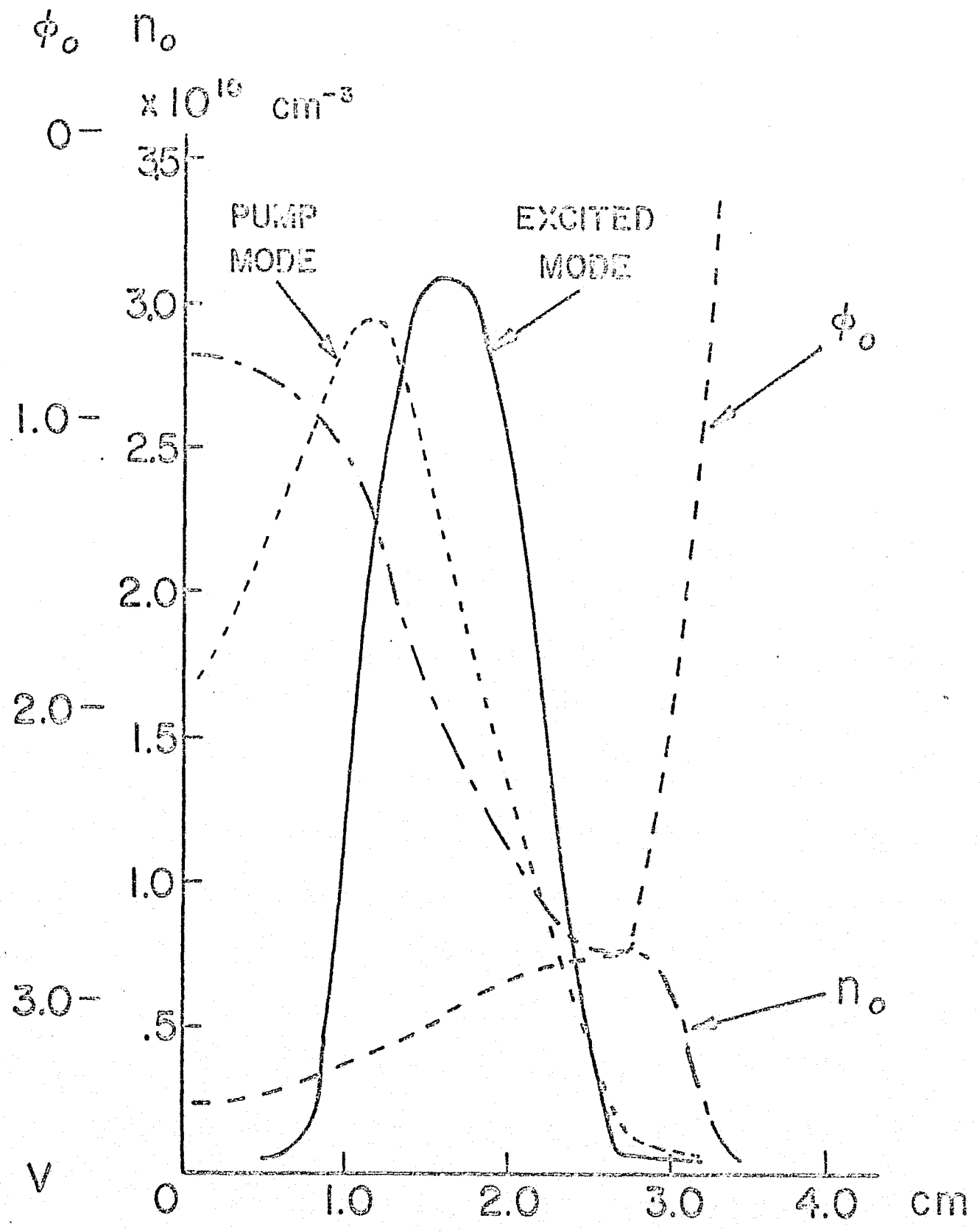
ϕ_o n_o
x 10^{16} cm^{-3}
0
3.5
3.0
2.5
2.0
1.5
1.0
.5
1.0
2.0
3.0
PUMP MODE
EXCITED MODE
ϕ_o
n_o
V
0
1.0
2.0
3.0
4.0
cm

FIG. 7

FIG. 5

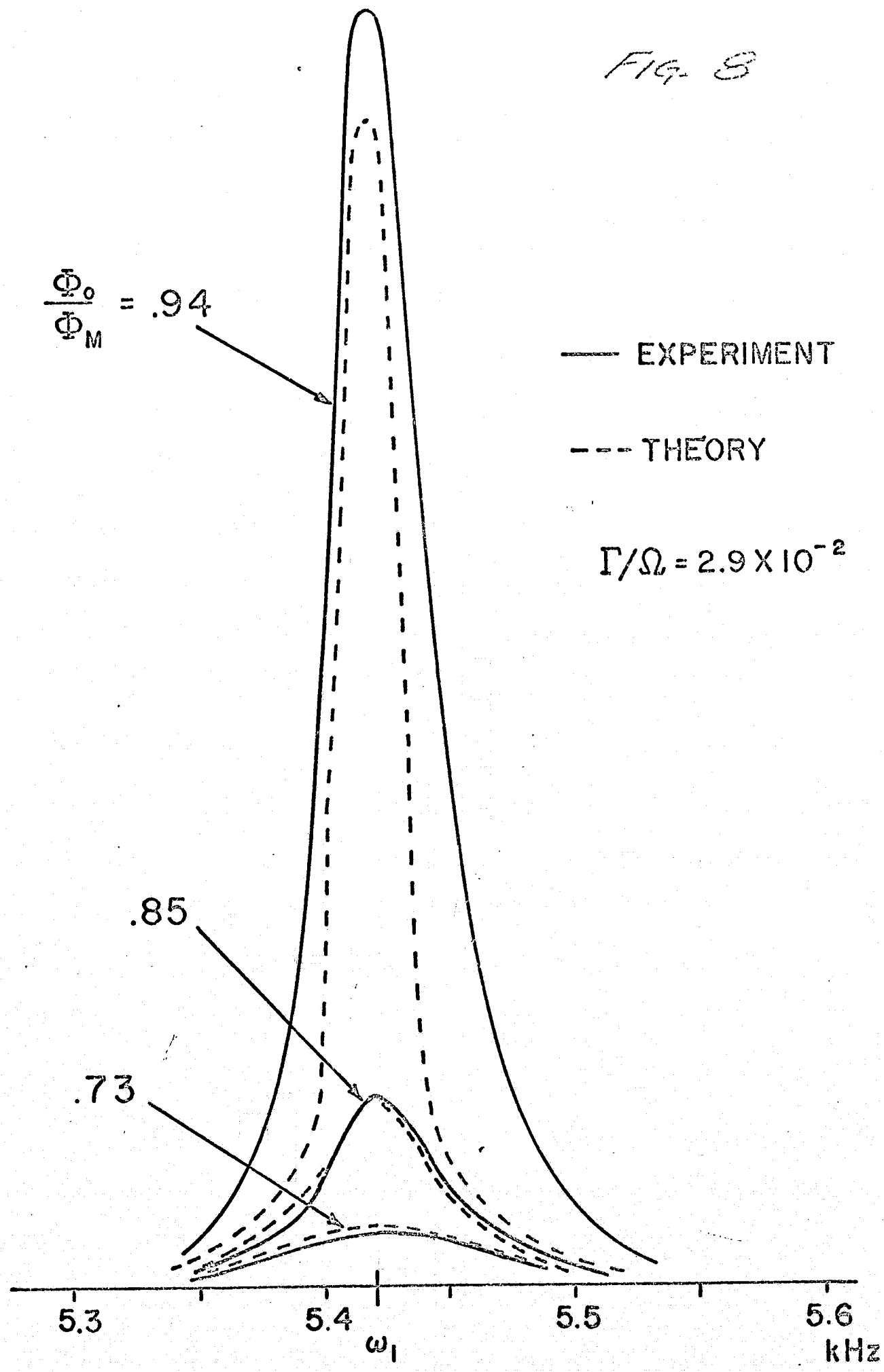
$\frac{\Phi_0}{\Phi_M}$ = .94
.85
.73
5.3
5.4
5.5
5.6
ω_1
kHz
EXPERIMENT
THEORY
$\Gamma/\Omega = 2.9 \times 10^{-2}$

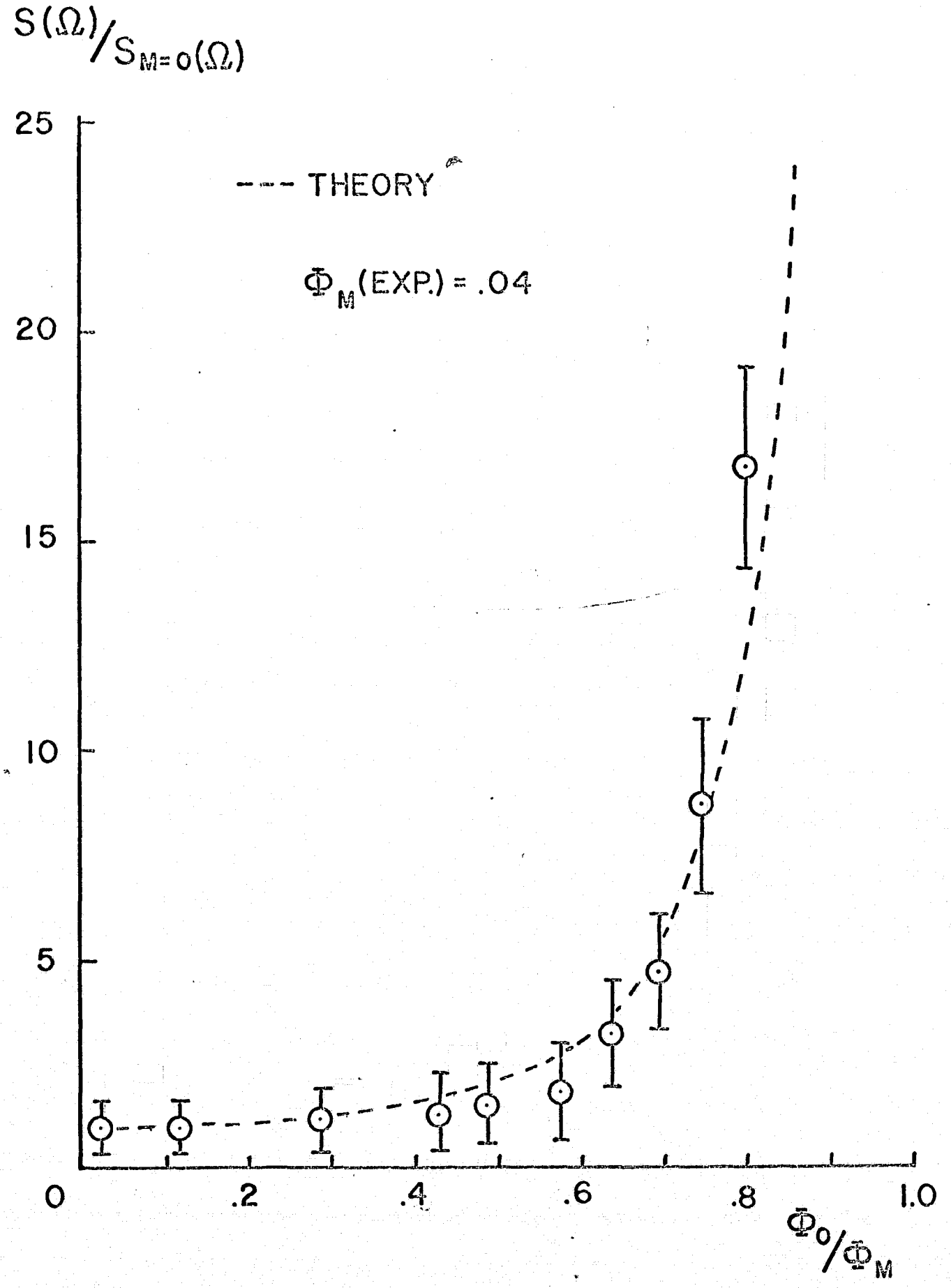
$S(\Omega)/S_{M=0}(\Omega)$
25
20
15
10
5
0
.2
.4
.6
.8
1.0
--- THEORY
Φ_M(EXP.) = .04
Φ_0/Φ_M

FIG. 9

FIG 9

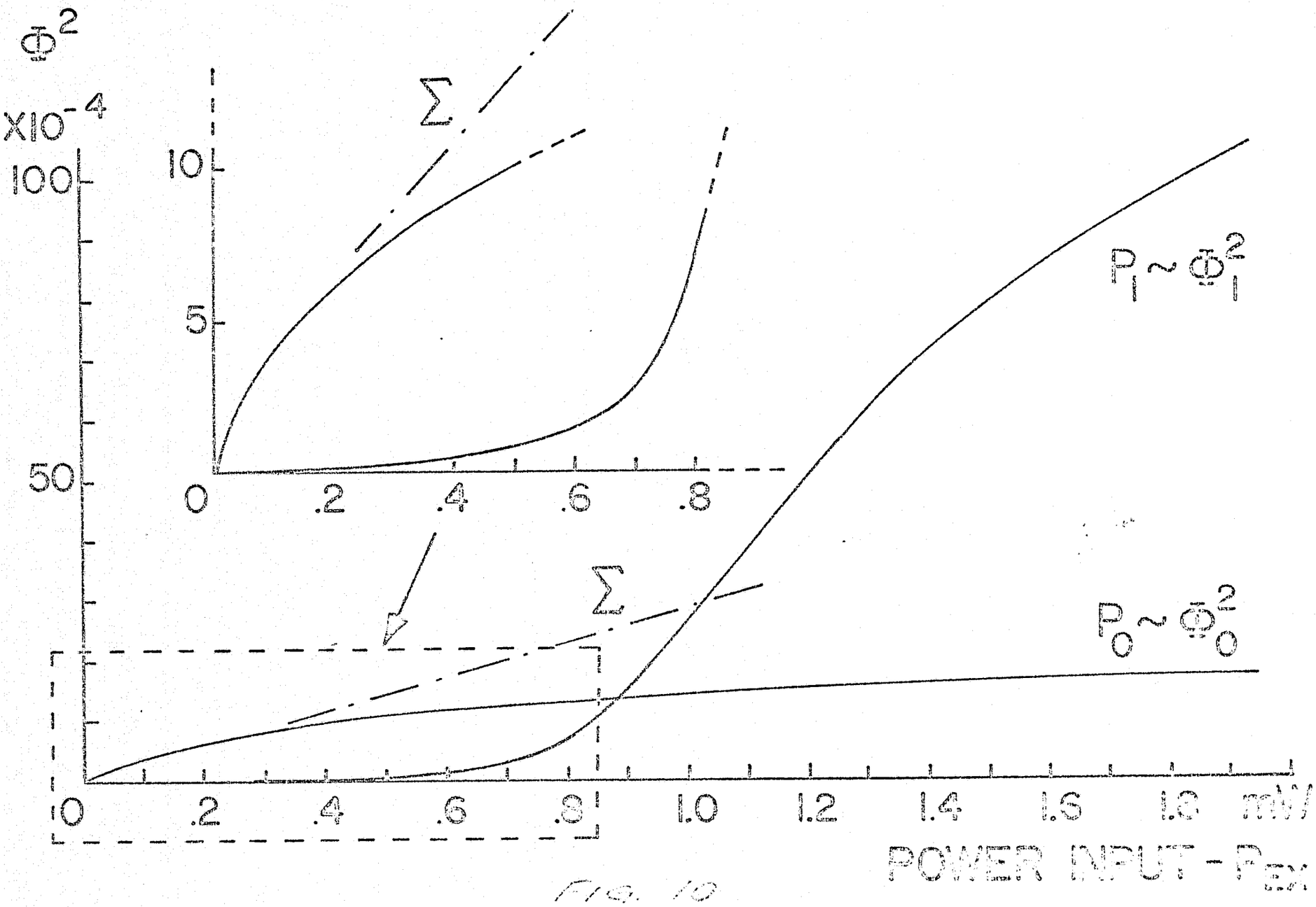
Φ^2
X10^{-4}
100
50
10
5
0
.2
.4
.6
.8
Σ
$P_I \sim \Phi_I^2$
$P_O \sim \Phi_O^2$
0
.2
.4
.6
.8
1.0
1.2
1.4
1.6
1.8
mW
POWER INPUT - P_{EX}

Fig. 10

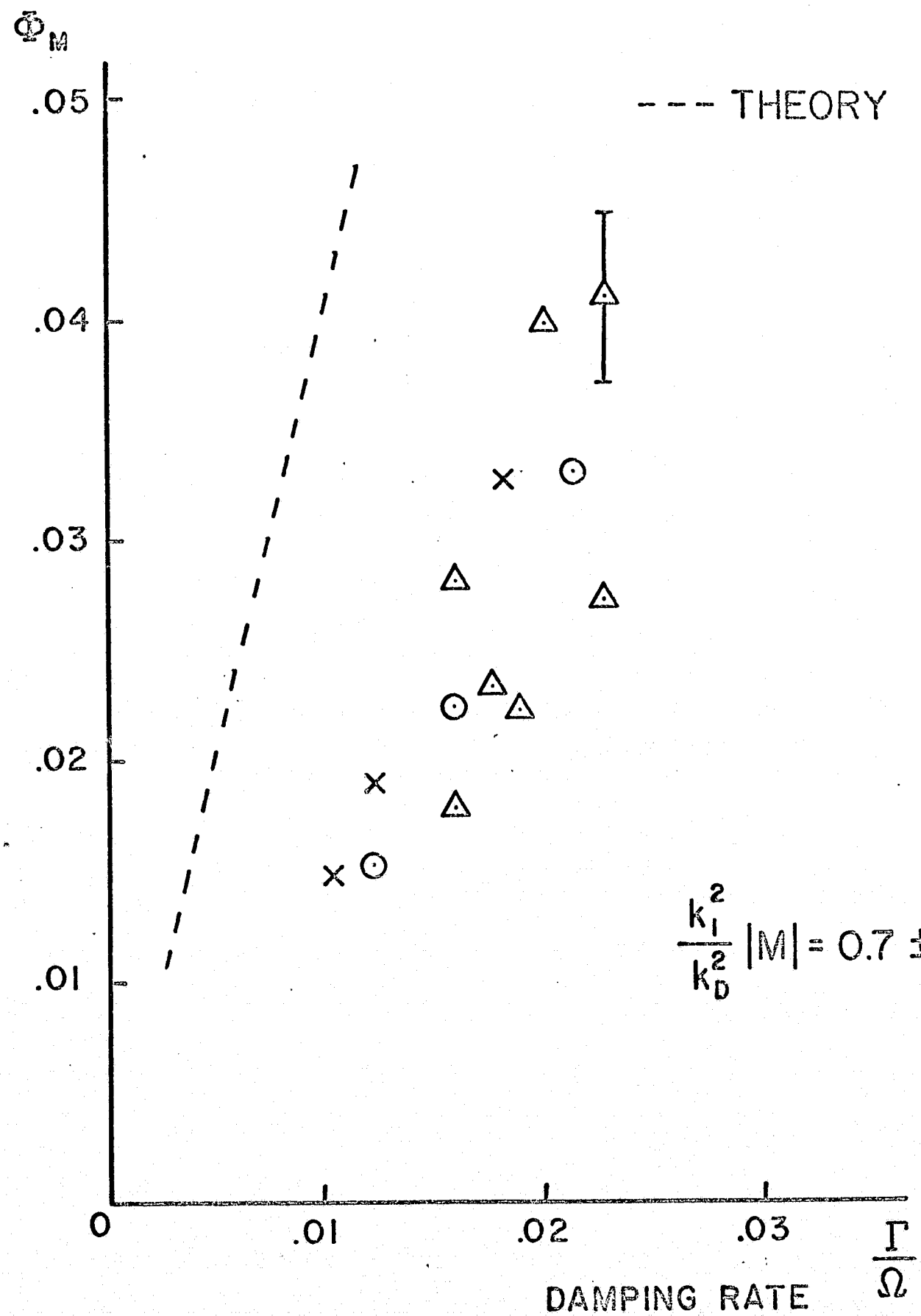
Φ_M
.05
.04
.03
.02
.01
0
.01
.02
.03
$\frac{\Gamma}{\Omega}$
DAMPING RATE
--- THEORY
$\frac{k_1^2}{k_D^2}|M| = 0.7 \pm .2$

FIG. 11

FIG. 11

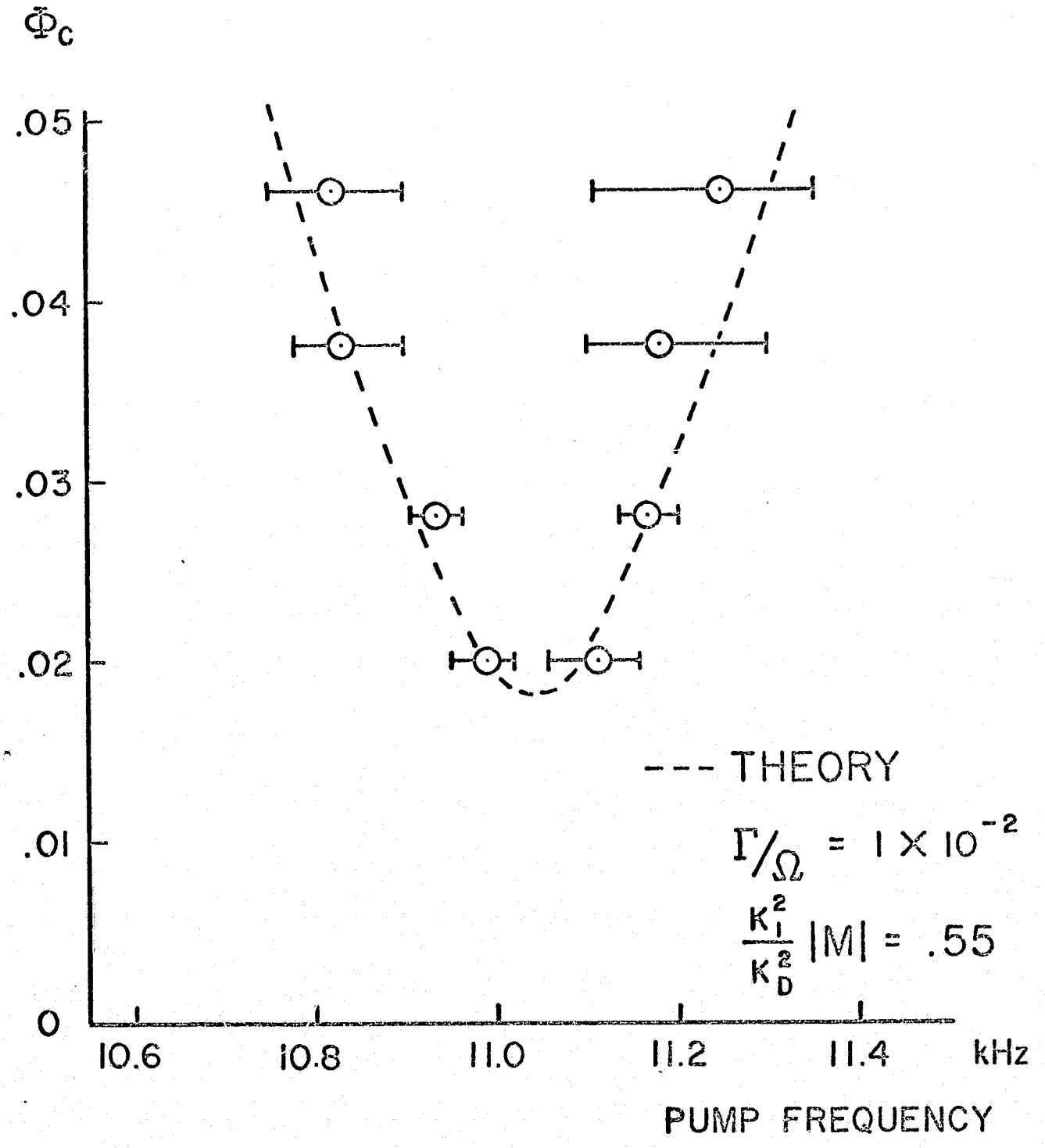
Φ_c
.05
.04
.03
.02
.01
0
10.6
10.8
11.0
11.2
11.4
kHz
PUMP FREQUENCY
--- THEORY
$\Gamma/\Omega = 1 \times 10^{-2}$
$\frac{K_1^2}{K_D^2}|M| = .55$

FIG. 12

FIG. 12

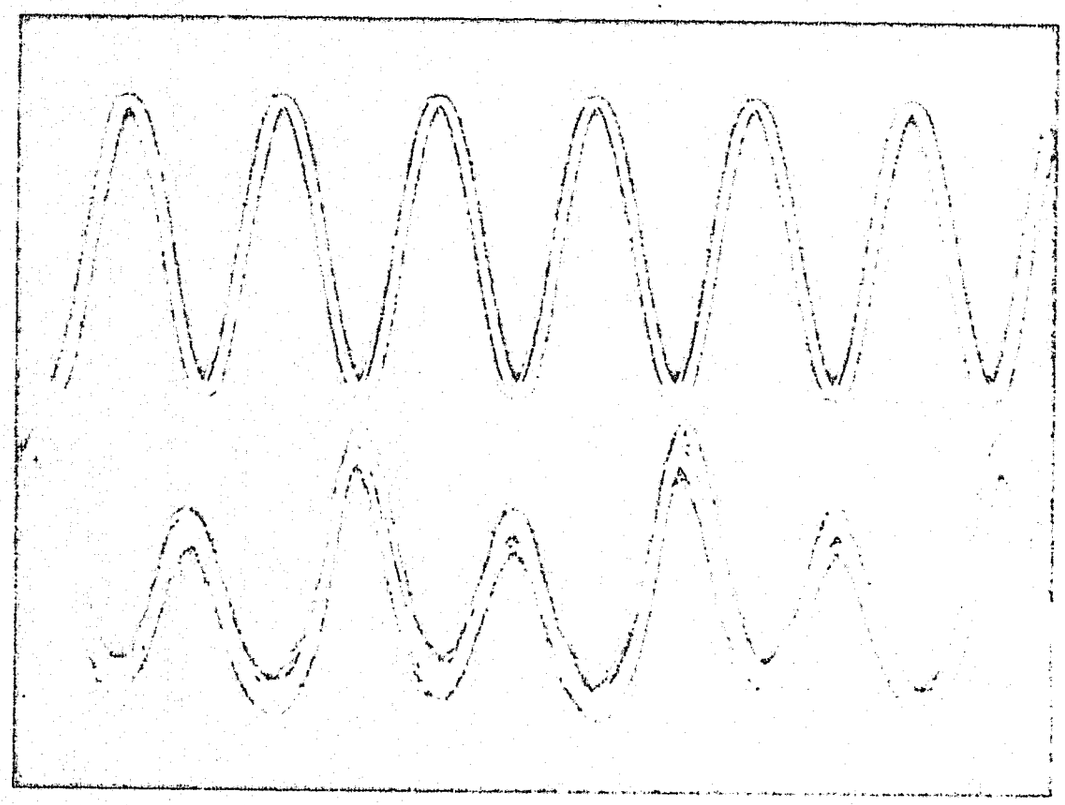

EXTERNAL PUMP – ω_0

PUMP WAVE – ω_0

and

EXCITED WAVE – ω_1

FIG. 13

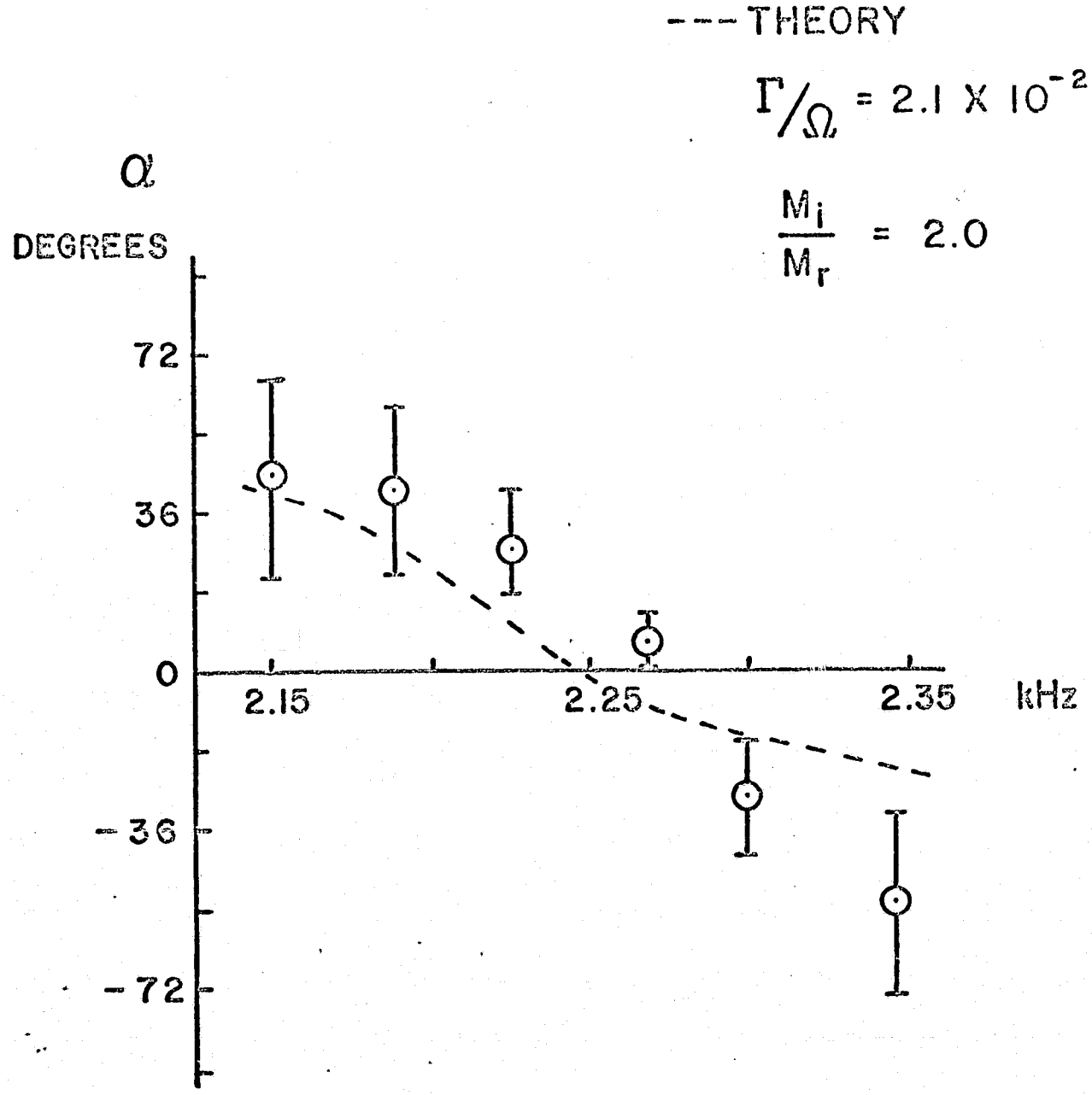
---THEORY
$\Gamma/\Omega = 2.1 \times 10^{-2}$
$\frac{M_i}{M_r} = 2.0$
α
DEGREES
72
36
0
-36
-72
2.15
2.25
2.35
kHz

FIG. 14

FIG. 14

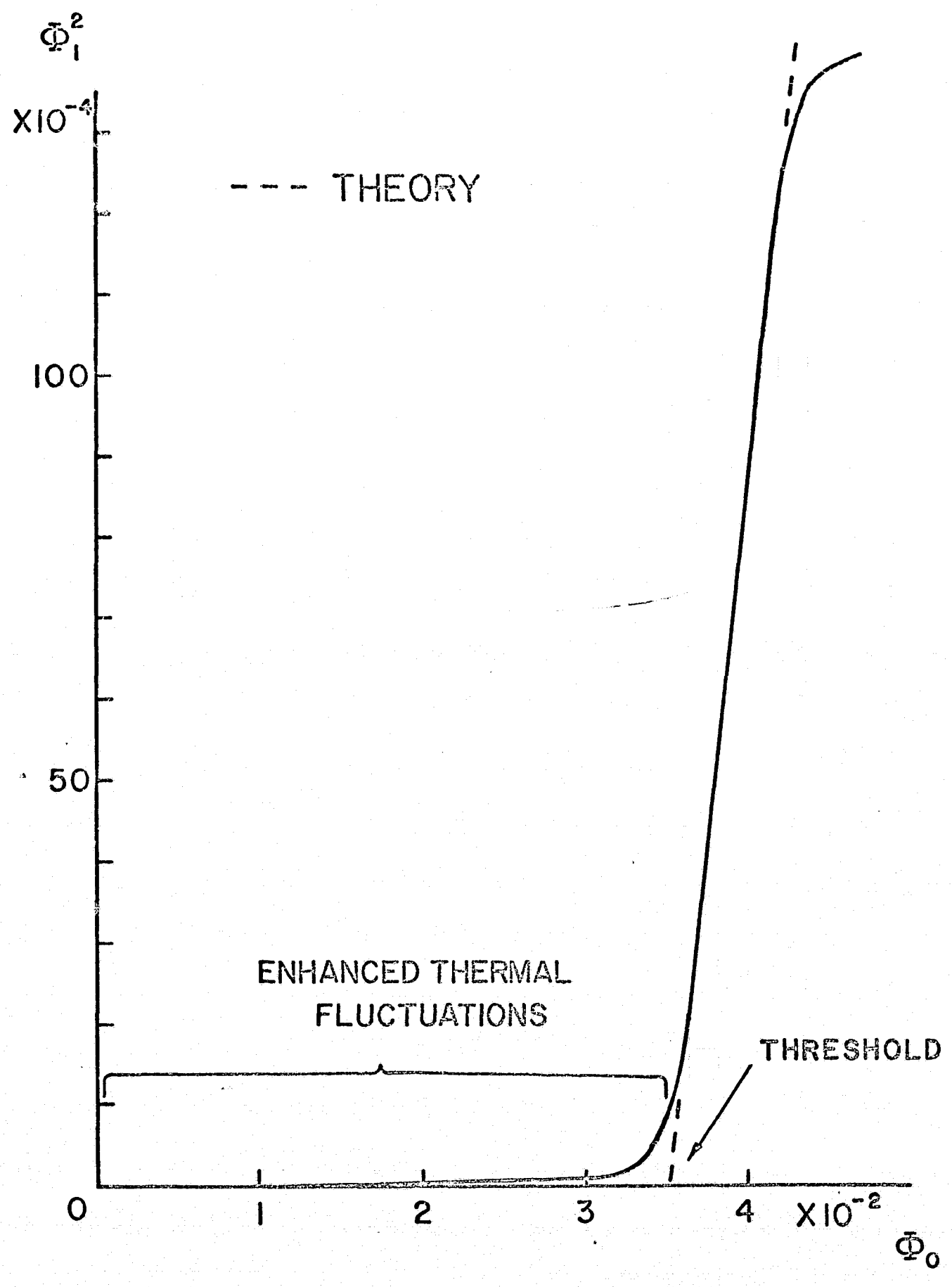
Φ_1^2
X10^{-4}
100
50
0
--- THEORY
ENHANCED THERMAL
FLUCTUATIONS
THRESHOLD
1
2
3
4
X10^{-2}
Φ_0

FIG. 15

FIG. 15

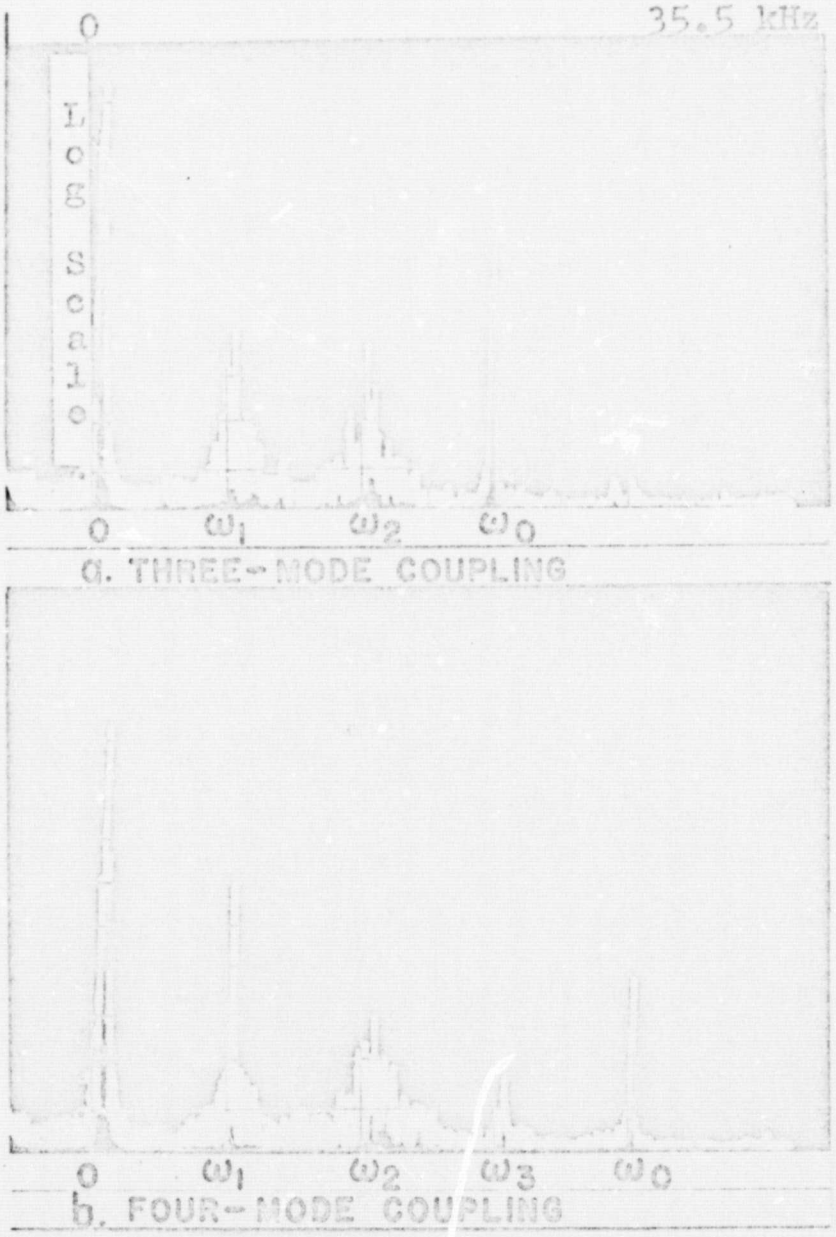
0
35.5 kHz
Log scale
0
ω_1
ω_2
ω_0
a. THREE-MODE COUPLING
0
ω_1
ω_2
ω_3
ω_0
b. FOUR-MODE COUPLING

FIG. 16

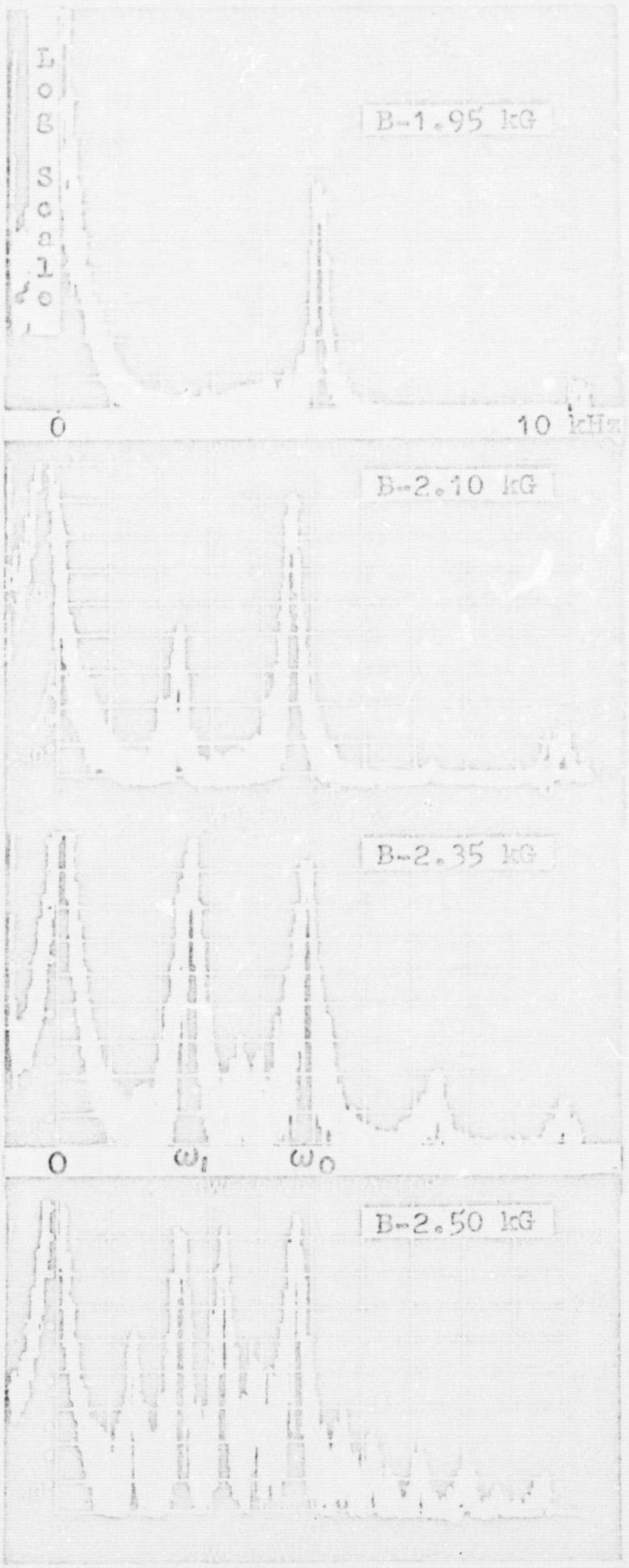

Fig. 17